Bulletin of the Seismological Society of America, Vol. 88, No. 6, pp. 1466–1483, December 1998

Conditions under which Velocity-Weakening Friction Allows a Self-healing versus a Cracklike Mode of Rupture

by Gutuan Zheng and James R. Rice

Abstract Slip rupture processes on velocity-weakening faults have been found in simulations to occur by two basic modes, the expanding crack and self-healing modes. In the expanding crack mode, as the rupture zone on a fault keeps expanding, slip continues growing everywhere within the rupture. In the self-healing mode, rupture occurs as a slip pulse propagating along the fault, with cessation of slip behind the pulse, so that the slipping region occupies only a small width at the front of the expanding rupture zone.

We discuss the determination of rupture mode for dynamic slip between elastic half-spaces that are uniformly prestressed at background loading level τ_0^b outside a perturbed zone where rupture is nucleated. The interface follows a rate and state law such that strength τ_{strength} approaches a velocity-dependent steady-state value $\tau_{ss}(V)$ for sustained slip at velocity V, where $d\tau_{ss}(V)/dV \leqq 0$ (velocity weakening). By proving a theorem on when a certain type of cracklike solution cannot exist, and by analyzing the results of 2D antiplane simulations of rupture propagation for different classes of constitutive laws, and for a wide range of parameters within each, we develop explanations of when one or the other mode of rupture will result. The explanation is given in terms of a critical stress level τ_{pulse} and a dimensionless velocity-weakening parameter T that is defined when $\tau_0^b \geqq \tau_{\text{pulse}}$. Here τ_{pulse} is the largest value of τ_0^b satisfying $\tau_0^b - (\mu/2c)V \leq \tau_{ss}(V)$ for all $V > 0$, where μ is the shear modulus and c is the shear wave speed. Also, $T = [-d\tau_{ss}(V)/dV]/(\mu/2c)$ evaluated at $V = V_{\text{dyna}}$, which is the largest root of $\tau_0^b - (\mu/2c)V = \tau_{ss}(V)$; $T = 1$ at $\tau_0^b = \tau_{\text{pulse}}$, and T diminishes toward 0 as τ_0^b is increased above τ_{pulse}.

We thus show that the rupture mode is of the self-healing pulse type in the low-stress range, when $\tau_0^b < \tau_{\text{pulse}}$ or when τ_0^b is only slightly greater than τ_{pulse}, such that T is near unity (e.g., $T > 0.6$). The amplitude of slip in the pulse diminishes with propagation distance at the lowest stress levels, whereas the amplitude increases for τ_0^b above a certain threshold τ_{arrest}, with $\tau_{\text{arrest}} < \tau_{\text{pulse}}$ in the cases examined. When τ_0^b is sufficiently higher than τ_{pulse} that T is near zero (e.g., $T < 0.4$ in our 2D antiplane simulations), the rupture mode is that of an enlarging shear crack.

Thus rupture under low stress is in the self-healing mode and under high stress in the cracklike mode, where our present work shows how to quantify low and high. The results therefore suggest the possibility that the self-healing mode is common for large natural ruptures because the stresses on faults are simply too low to allow the cracklike mode.

Introduction: Self-healing Pulse versus Cracklike Slip Rupture Mode

Computational simulations (Cochard and Madariaga, 1994, 1996; Perrin *et al.*, 1995; Beeler and Tullis, 1996) have shown that dynamic slip on homogeneous velocity-weakening faults may occur by either an enlarging crack mode or a self-healing slip pulse mode. Our goal here is to establish conditions, in terms of applied loading and features of the constitutive response, under which one or the other mode occurs. The study is for slip on the interfacial fault, on the plane $y = 0$, between two identical elastic half-spaces. In the most general 3D circumstances, the slip δ varies with both coordinates in the fault plane, $\delta = \delta(x, z, t)$. We develop some general results for that 3D context, but

the specific numerical simulations reported are done for the 2D antiplane case, in which slip is constrained to be in the z direction, and to be uniform in z, so that $\delta = \delta(x, t)$. Frictional constitutive properties are taken as uniform along the fault.

A classification of the rupture modes may be given as follows. Suppose that a rupture process is nucleated on a portion of a fault that is uniformly loaded outside that nucleation zone and that the rupture still continues somewhere on the fault after an arbitrarily long time. Then two things can happen at that nucleation portion: (1) Slip is completely arrested, so that the slipping patch is split into two in the 2D case (or into an annular zone in the 3D case). It is then plausible to expect that arresting signals from the nucleation portion are sent out, and the fault heals behind the rupture fronts, therefore resulting in traveling slip pulses propagating away from the nucleation portion and a self-healing mode of rupture. (2) Slip in the nucleation portion persists, resulting in a cracklike rupture mode. In this case, the maximum velocity is associated with the rupturing front, and each position on the fault, once triggered, continues to slip, exhibiting an indefinitely enlarging crack.

The cracklike rupture mode has been widely observed in numerical simulations. These include cases of prescribed uniform strength drop on the fracture surface in models with singularities at the rupture front (e.g., Kostrov, 1966; Madariaga, 1976; Freund, 1979; Day, 1982) or with nonsingular slip weakening (e.g., Ida, 1972; Andrews, 1976a,b, 1985; Harris and Day, 1993). There is, however, a paucity of results in the early literature that display the self-healing rupture mode. Other than being due to the simplicity of rupture models, such absence relates to the relatively recent focus on the shortness of rupture duration, principally due to Heaton (1990), which he argues to be required by inversions that fit slip histories to the high-frequency seismic signals sent out from propagating ruptures. Theoretical and simulation studies of conditions leading to self-healing pulses,in models that include velocity weakening of friction strength, have been given by Cochard and Madariaga (1994, 1996), Perrin *et al.* (1995), and Beeler and Tullis (1996). Still, not all velocity-weakening models lead to self-healing. For example, dynamic simulations of Okubo (1989), Rice and Ben-Zion (1996), and Ben-Zion and Rice (1997) based on the classical logarithmic dependence on slip velocity, as extrapolated from much lower-speed laboratory experiments, showed the cracklike mode. This study shows why such results occur and also that for a given velocity-weakening law, the self-healing rupture mode occurs at a lower stressing level than the cracklike mode, and the slip magnitude is, correspondingly, much smaller. Further, as Perrin *et al.* (1995) proved, a steadily propagating slip pulse in the self-healing mode can exist only if the constitutive relations allow for ageing, that is, for restrengthening of the fault in stationary contact. The self-healing mode has been proposed as a mechanism that may seal in complex stress distributions on the fault after each rupture (Cochard and Madariaga, 1996).

Heaton found that the slip duration, derived as the dislocation rise time, is only of the order of about 10% of the overall duration of the earthquake. He argued that the rupture mode on the fault surface is in the form of a self-healing pulse. Further, he postulated that the slip pulse is possible if the friction weakens with the slip rate. This conforms with the Brune (1976) idea that a pulse may exist if the fault strength is low immediately behind the rupture front and builds up quickly at finite distance from the front. Heaton (1990) also cited a model by Freund (1979) to show that a healing slip pulse, which causes a finite dislocation, can propagate at a constant velocity within an unbounded solid. The Freund model, which envisions spatially uniform friction strength on the fault during slip, requires that the healed portion sustain greater stress than it did immediately before, while slipping.

Although our purpose here is to investigate the relation between velocity-weakening friction and short-duration slip pulses due to self-healing, it is important to understand that other mechanisms exist. One involves geometric confinement of the rupture domain by unbreakable regions. Day (1982) found such pulselike behavior in his 3D numerical elastodynamic rupture models with constant stress drop, when the rupture process was confined within a long but narrow region by unbreakable barriers (the formulation would lead to a cracklike mode in the absence of barriers). He observed that the rupture starts in a classical cracklike mode near the epicenter and propagates in all directions but that arresting signals come in from the borders that effectively relock the fault behind the rupture front, and the result is two slip pulses. Johnson (1992) studied faulting in a 2D model of a brittle crustal plate that is coupled to a nonbrittle substrate and found slip-pulse generation by a similar mechanism to that of Day. Johnson (1990) also studied rupture in models without the feature of confinement of slip to a narrow channel; he noticed that if the rupture initially propagates bilaterally and is then arrested by a strong barrier at one end, the healing wave, combined with the propagation of the other end, forms a pulselike rupture pattern. Perrin *et al.* (1995) also illustrate this barrier-based mechanism of self-healing in a case that would, otherwise, result in cracklike rupture.

Beroza and Mikumo (1996) re-examined the 1984 Morgan Hill, California, earthquake using strong-motion data. They suggested that spatially heterogeneous fault strength, in absence of any significant velocity weakening at slip rates during rupture, may control the rupture behavior and give rise to the short-duration slip pulse. By using a velocity-independent failure model, they inverted for the heterogeneous distribution of a (grid-sensitive) stress increase needed to initiate slip and stress drop describing strength after initiation, so that results of a spontaneous dynamic rupture analysis would give a slip history consistent with what had been obtained by an earlier kinematic inversion of the strong-motion data. Their results show confinement of rapid slip to the vicinity of the rupture front. Apparently, the strong heterogeneities generate local arrest waves analogous

to those of Day (1982) and Johnson (1990, 1992) discussed earlier. Recently, Olsen *et al.* (1997) also reported such behavior in a slip-weakening model of the 1992 Landers, California, earthquake, and Day *et al.* (1998) reported similar results for that event as well as for the 1994 Northridge and 1995 Kobe earthquakes.

Another mechanism for self-healing pulse generation, even in the absence of velocity or displacement dependence of friction, relates to the possible moderate dissimilarity of material properties across a fault plane. Andrews and Ben-Zion (1997) found a dynamic slip pulse on a fault of constant Coulomb friction coefficient when the interface separates materials of different elastic properties and densities, noting that such an effect had been suggested much earlier by Weertman (1980) based on his analysis of steadily moving interfacial dislocations. The effect occurs for in-plane slip, which couples to alteration of normal stress when there is material dissimilarity. The difference in material induces different normal stress polarities, and slip effectively occurs only in a narrow region where the large dynamic normal stress variations weaken the resistance to shearing. Such effects have also been studied by Harris and Day (1997), who emphasize that it may come into play also for slippage along the border between a compliant fault core and surrounding crustal rock. The effect is related to the remarkable recent discovery by Adams (1995) that steady-state sliding along the interface of two elastic half-spaces of different material properties is unstable to perturbation, in the sense that the real parts of eigenvalues, for exponential time dependence of a Fourier spatial perturbation, are positive for a very broad range of material pairs and friction coefficients. Subsequently, Adams (1998) showed that pulses of constant slip velocity can move at a generalized Rayleigh speed along such dissimilar material interfaces, with constant friction coefficients, under remotely applied shear stress levels that are arbitrarily less than the friction strength based on the remotely applied normal stress, an effect that Rice (1997) has shown to follow simply from the Weertman (1980) analysis.

Thus, there are other plausible candidate mechanisms, in addition to the velocity-weakening mechanism, for self-healing slip pulses, and it is important to learn more about the characteristics of each. In this article, we conduct an analysis of a homogeneous velocity-weakening fault embedded between two identical elastic half-spaces, and develop new criteria to classify the fault-rupture modes. Then we investigate by simulations, for the 2D antiplane case, the stress and slip variations for specific types of velocity-weakening laws and for a broad range of parameters in each, thus illustrating the rupture mode selection and providing confirmation of the theoretical work.

Elastodynamic Representation and Background Loading

The elastodynamic interactions between the fault surface and its elastic surroundings require that the slip $\delta(x, z, t)$, slip rate $V(x, z, t) = \partial\delta/\partial t$, and shear stress $\tau(x, z, t)$ in the slip direction be related by

$$\tau(x,z,t) = \tau_0(x,z,t) + \phi(x,z,t) - \frac{\mu}{2c} V(x,z,t). \quad (1)$$

The first term, $\tau_0(x, z, t)$, denotes the loading condition, that is, the stress that would be sustained if the fault were constrained against any slip. The last term represents radiation damping (Rice, 1993), where μ is the elastic rigidity and c is the shear wave speed. The middle term $\phi(x, z, t)$ is a linear functional of $\delta(x', z', t')$ for all x', z', t' within the elastodynamic wave cones with apex at x, z, t. Cochard and Madariaga (1994) introduced such a function $\phi(x, t)$ for the 2D antiplane case and expressed it as a space–time convolution integral on slip $\delta(x', t')$ for all x', t' satisfying $c(t - t') > |x - x'|$. Later, Perrin *et al.* (1995) introduced a spectral representation of $\phi(x, t)$ in that 2D case, which we adopt for our simulations here and briefly outline in Appendix 1. In the general 3D context, the spectral representation of $\phi(x, z, t)$ is given by Geubelle and Rice (1995) and a space–time convolution integral representation is given by Cochard and Rice (1997a) and by Fukuyama and Madariaga (1998). Earlier 2D and 3D integral representation of elastodynamic response (e.g., Andrews, 1976a,b, 1985; Das, 1980; Das and Kostrov, 1987) can be expressed in a form that similarly extracts the instantaneous response term $-\mu V/2c$ to leave a functional ϕ as above.

We take the loading $\tau_0(x, z, t)$ for $t > 0$ to be uniform at a background loading level τ_0^b, except that we perturb that uniform level in some small region as required to nucleate a rupture. Thus, for example, in our 2D simulations,

$$\tau_0(x,t) = \begin{cases} \tau_0^b & \text{for } t < 0 \\ \tau_0^b + \tau_0^p(x) & \text{for } t > 0' \end{cases} \quad (2)$$

where $\tau_0^p(x)$ is a perturbation term that acts over a localized zone so as to nucleate the rupture. We use a simple boxcar perturbation (Fig. 1) like in Perrin *et al.* (1995).

Two properties of the functional $\phi(x, z, t)$ are important to the subsequent theorem on when certain types of solutions are disallowed. The first property is that the part of the stress represented by ϕ is conserved, that is, shifted from place to place by waves but not created or destroyed:

$$\int_{-\infty}^{+\infty}\int_{-\infty}^{+\infty} \phi(x,z,t)dxdz = 0 \quad \text{for all slip histories } \delta(x,z,t). \quad (3)$$

This is derived once we realize that the integral is the Fourier transform, $\tilde{\phi}(k, m, t)$, of $\phi(x, z, t)$ at wavenumbers $k = m = 0$; Geubelle and Rice (1995) show that $\tilde{\phi}(k, m, t)$ is given by a convolution on time of a certain function with $\tilde{\delta}(k, m, t)$ and that function vanishes identically when $k = m = 0$.

The corresponding 2D antiplane result follows similarly and is

$$\int_{-\infty}^{+\infty} \phi(x,t)dx = 0 \quad \text{for all slip histories } \delta(x,t). \tag{4}$$

The second property refers to the functional ϕ in response to a state of spatially uniform slip, $\delta(x, z, t) = \delta(t)$ for all t, and is

$$\phi(x,z,t) = 0 \quad \text{when } \delta(x,z,t) = \delta(t). \tag{5}$$

To see why, note that in this case, the walls of the fault displace by $u(x, 0^+, z, t) = \delta(t)/2$ and $u(x, 0^-, z, t) = -\delta(t)/2$, where u is the fault-parallel displacement component. The requisite governing equations in the adjoining half-spaces are then met if $u(x, y, z, t) \equiv u(y, t)$ satisfies $c^2\partial^2u/\partial y^2 = \partial^2u/\partial t^2$, with solution $u(y, t) = \delta(t - y/c)/2$ in $y > 0$, $u(y, t) = -\delta(t + y/c)/2$ in $y < 0$. The stress alteration, corresponding to $\tau - \tau_0$, associated with these waves is $\mu\partial u/\partial y$ at $y = 0$ (the result is continuous as $y \to 0^+$ and 0^-), which is just $-\mu\dot{\delta}(t)/2c = -\mu V(t)/2c$. Thus, comparison with equation (1) shows that $\phi = 0$ in this case. This discussion follows an explanation of the origin of the radiation damping factor given by Rice (1993).

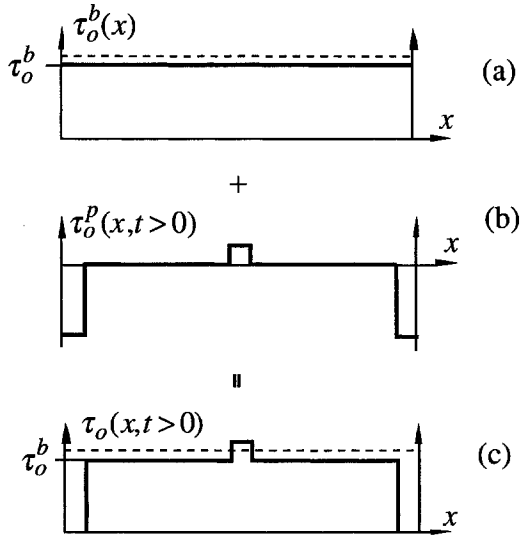

Figure 1. (a) Uniform background loading τ_0^b on a fault. (b) Perturbation $\tau_0^p(x,t > 0)$ used to nucleate a rupture in the numerical simulations shown subsequently. The simulations also included a decrease of stress at the ends of a segment to form barriers that ultimately stop the rupture, although we do not discuss stopping effects here. (c) Net loading stress $\tau_0(x,t > 0)$ prevailing for simulated ruptures. The dashed line represents an exactly or approximately defined stress level above which rapid slip will initiate.

Velocity-Weakening Constitutive Laws in the Rate- and State-Dependent Framework

We introduce specific constitutive laws later for use in the 2D simulations. Here, general properties are of interest. We consider situations of slip under constant effective normal stress. In that case, the strength is given by an equation of the form

$$\tau_{\text{strength}} = F(V,\theta) \tag{6}$$

where $\partial F(V,\theta)/\partial V > 0$, and where θ is a state variable that evolves during the slip history and represents, for example, the average age of the current population of asperity contacts. To complete the constitutive framework, a state evolution equation of form

$$d\theta/dt = G(V,\theta) \tag{7}$$

is introduced (a commonly used form is the Dieterich-Ruina ageing, or slowness, law, in which $G \equiv 1 - V\theta/L$, where L, sometimes called d_c, is a characteristic sliding distance for renewal of the population of asperity contacts). It is assumed that for fixed V, solutions of (7) evolve toward a steady-state value $\theta_{ss} = \theta_{ss}(V)$, which is the solution of

$$G(V,\theta_{ss}) = 0. \tag{8}$$

Further, the steady-state strength is

$$\tau_{\text{strength}} = \tau_{ss}(V) \equiv F[V,\theta_{ss}(V)], \tag{9}$$

and we assume, for the cases of interest here, that $d\tau_{ss}(V)/dV < 0$ (velocity weakening). Features of such response are illustrated in Figure 2, for which the heavy line shows the steady-state strength and the light lines the variations of strength when the sliding velocity is suddenly changed from that of a steady-state at V_1 to some new velocity V_2. The slip distance L for state evolution is defined such that

$$d\theta/dt \approx -(V/L)\,[\theta - \theta_{ss}(V)] \tag{10}$$

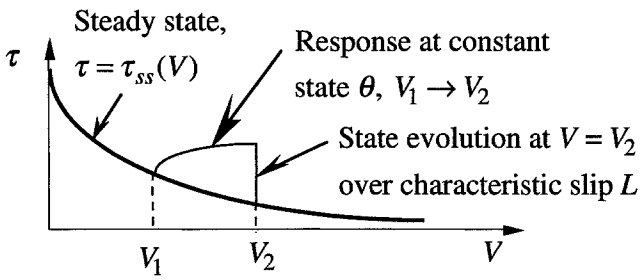

Figure 2. Illustration of friction law. Heavy line shows steady-state strength. Light lines show response when slip rate V is changed suddenly (i.e., at constant state θ) from V_1 to V_2.

for θ near $\theta_{ss}(V)$. Using (7), and subtracting from it the equation $0 = G[V, \theta_{ss}(V)]$, one sees from

$$d\theta/dt = G(V,\theta) - G[V,\theta_{ss}(V)] \approx [\partial G(V,\theta)/\partial\theta]_{\theta=\theta_{ss}(V)}[\theta - \theta_{ss}(V)] \quad (11)$$

that the formal definition of $L[=L(V)]$ is

$$L = -V/[\partial G(V,\theta)/\partial\theta]_{\theta=\theta_{ss}(V)}. \quad (12)$$

This is consistent with L in the Dieterich–Ruina ageing law.

The distance L as measured in laboratory friction studies generally falls into the range of 1 to 100 μm (and most often of order 5 to 10 μm). It is much smaller than slips during ruptures that will be of interest to us, and one might wish to ignore the entire state evolution process, set $L = 0$, and just write $\tau_{\text{strength}} = \tau_{ss}(V)$, which is a pure velocity-weakening law. However, various studies of frictional stability and rupture dynamics for sliding between elastic continua (Rice and Ruina, 1983; Dieterich, 1992; Rice, 1993; Perrin *et al.*, 1995; Rice and Ben-Zion, 1996) suggest that problems may not be well posed if we set $L = 0$. Further, Perrin *et al.* (1995) showed that self-healing rupture solutions, as steadily propagating slip pulses between elastic half-spaces, do not exist for pure velocity-weakening laws but rather require some feature of state evolution so that τ_{strength} can increase at least moderately with time on the relocked part of the fault. Also, the state evolution features allow for effects like a finite fracture energy near the rupture tip (analogously to the way slip-weakening models correspond to a fracture energy; Ida, 1972; Palmer and Rice, 1973), so that the rupture speed can be less than the shear wave speed for antiplane strain or less than the Rayleigh speed for in-plane strain. So we include the state evolution features of the laboratory-based rate- and state-dependent description of velocity weakening here.

Nevertheless, for a well-developed cracklike rupture, with slips δ that are much larger than L, the analysis by Rice and Tse (1986) of inertia-controlled dynamic instability within the rate and state framework shows that the constitutive law will give $\tau_{\text{strength}} \approx \tau_{ss}(V)$ everywhere except near the rupture tip, at least when slip rates satisfy $L/V \ll V/|\dot{V}|$. That is because L/V is a characteristic time for state to evolve toward $\theta_{ss}(V)$ and strength toward $\tau_{ss}(V)$, whereas $V/|\dot{V}|$ is a characteristic time over which the targets, $\theta_{ss}(V)$ and $\tau_{ss}(V)$, for the state evolution change. Hence, if $L/V \ll V/|\dot{V}|$, or if $|\dot{V}|L/V^2 \ll 1$, there is enough time to evolve toward what are essentially steady-state conditions associated with the instantaneous V, and $\tau_{\text{strength}} \approx \tau_{ss}(V)$. If a particular point on the cracklike rupture considered has been slipping for a time t, then we may roughly estimate $|\dot{V}|$ as V/t. Hence, at positions on the rupture for which $L/Vt \ll 1$, which essentially means positions for which $L/\delta \ll 1$ (where δ is slip at that location), we will have $\tau_{\text{strength}} \approx \tau_{ss}(V)$. This region includes all the rupture except for small regions, of a size that scales with L, near the tip in which a state evolution process analogous to slip-weakening takes place. This feature of the cracklike rupture mode is important, as now seen, to understanding conditions under which the cracklike mode cannot occur.

Understressing and Impossibility of the Cracklike Rupture Mode for Background Loading below τ_{pulse}

An important range of understressing is defined as that for which the background loading τ_0^b is less than a critical stress level that we call τ_{pulse}. Here τ_{pulse} is the maximum value of τ_0^b that satisfies

$$\tau_0^b - (\mu/2c)V \le \tau_{ss}(V) \quad \text{for all } V \ge 0. \quad (13)$$

The τ_{pulse} thus defined is illustrated in Figure 3a, which also shows the line $\tau = \tau_0^b - (\mu/2c)V$ for a $\tau_0^b < \tau_{\text{pulse}}$.

We now argue that no rupture solution in the form of an indefinitely expanding crack can exist when $\tau_0^b < \tau_{\text{pulse}}$. The precise theorem we prove is this: Let $S_{\text{out}}(t)$ be the part of the interface $y = 0$ between half-spaces that lies outside the slipping region of a tentatively hypothesized cracklike rupture solution at time t. Then we prove that no solution can exist, when $\tau_0^b < \tau_{\text{pulse}}$, with the property

$$\iint_{S_{\text{out}}(t)} [\tau(x,z,t) - \tau_0^b]dxdz \ge 0. \quad (14)$$

That is, no solution that increases (or fails to decrease) the shear force sustained by unruptured material outside the crack can actually exist. In the 2D case, the analogous property is

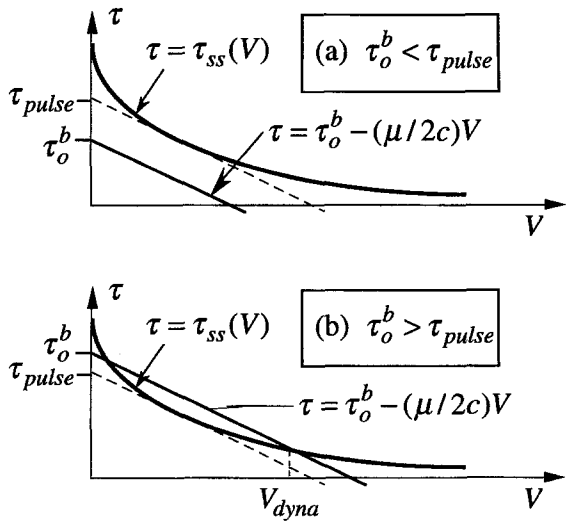

Figure 3. (a) Relative position of the radiation damping line $\tau = \tau_0^b - (\mu/2c)V$ and the steady-state friction $\tau = \tau_{ss}(V)$ for the understressing condition, $\tau_0^b < \tau_{\text{pulse}}$. (b) Relative position for $\tau_0^b > \tau_{\text{pulse}}$; the highest velocity intersection defines V_{dyna}.

$$\int_{S_{out}(t)} [\tau(x,t) - \tau_0^b]\, dx \geqq 0. \tag{15}$$

One commonly thinks of cracklike ruptures as shifting force onto the uncracked prolongation of the rupture zone, so that inequality (14) or (15) might be assumed to be a property of any crack solution. (Of course, the integrand of (14) and (15) vanishes at points beyond where waves have yet carried alterations of stress.) However, we emphasize that we have been able to rigorously prove that (15) holds for all possible crack solutions only in the antiplane case. See the discussion in Appendix 2.

Let us tentatively hypothesize, then, that an indefinitely expanding crack solution exists, radiating stresses ahead of it that satisfy (14) or (15). We will now observe that if $\tau_0^b < \tau_{pulse}$, the hypothesized solution violates (3) and hence cannot actually exist. To see this, observe from (1) that the functional ϕ must always meet

$$\phi(x,z,t) = \tau(x,z,t) - \tau_0^b + (\mu/2c)V. \tag{16}$$

In the region $S_{out}(t)$ lying outside the ruptured region at time t, $V = 0$, and so the property (14) implies that

$$\int\int_{S_{out}(t)} \phi(x,z,t)dxdz \geqq 0. \tag{17}$$

Now, as the crack becomes large so that slip satisfies $\delta \gg L$ everywhere except for the small regions of rapid state evolution near the rupture front, the stress is $\tau \approx \tau_{ss}(V)$, as explained earlier, and so (16) gives

$$\phi \approx \tau_{ss}(V) - [\tau_0^b - (\mu/2c)V]. \tag{18}$$

However, by our definition of τ_{pulse} (see Fig. 3), the quantity on the right is positive when $\tau_0^b < \tau_{pulse}$, so that $\phi > 0$ on the zone $S_{rupt}(t)$, which has been engulfed by the hypothesized cracklike rupture at time t. Thus,

$$\int\int_{S_{rupt}(t)} \phi(x,z,t)dxdz > 0. \tag{19}$$

This statement ignores that τ differs from $\tau_{ss}(V)$ within the state evolution zone. However, because that zone is of a size that is determined by L and does not increase as the rupture enlarges, it ultimately makes a negligible contribution to the total integral over S_{rupt}. Further, the nature of the constitutive description, with $\partial F(V, \theta)/\partial V > 0$, is such that τ increases substantially over $\tau_{ss}(V)$ in the region of rapidly accelerating slip at the tip of the rupture, so ϕ is even larger than the value in (18) and thus also contributes values $\phi > 0$ to the integral.

By combining (17) and (19), and recognizing that $S_{rupt} + S_{out}$ constitutes the entire plane between the half-spaces, we have that the integral of ϕ over the plane must be positive if the hypothesized cracklike rupture solution exists. But we know that ϕ must integrate to zero, as in (3). Hence, there is a contradiction, and the hypothesized solution cannot exist. An analogous argument applies to the 2D case.

Thus, rupture solutions in the form of indefinitely growing shear cracks cannot occur when $\tau_0^b < \tau_{pulse}$. Again, precisely this theorem rules out cracklike rupture solutions that satisfy (14) or (15). We have not been able to eliminate for all circumstances (i.e., other than the antiplane case) the possible existence of some anomalous rupture solution that somehow violated (14) or (15) and decreased the total shear force carried outside the ruptured zone, although we are unaware of any such solution ever being found.

Parameter T Characterizing Response for Background Loadings above τ_{pulse}

Suppose now that the background loading $\tau_0^b > \tau_{pulse}$, like for the higher loading level in Figure 3b. Then, if we assume that $\tau_{ss}(V) \geqq 0$, the equation

$$\tau_{ss}(V) = \tau_0^b - (\mu/2c)V \tag{20}$$

has at least one solution for V, and we denote by V_{dyna} the largest such solution (Fig. 3b). We may observe that $V = V_{dyna}$ and $\tau = \tau_{ss}(V_{dyna})$ is the solution for steady-state sliding under spatially uniform slip everywhere on the interface, because then $\tau = \tau_{ss}(V)$ and, from (5), $\phi = 0$ so that (1) reduces to (20). We prove in Appendix 3 that the solution at V_{dyna}, which necessarily satisfies

$$\mu/2c + [d\tau_{ss}(V)/dV]_{V=V_{dyna}} > 0, \tag{21}$$

is a stable solution for spatially uniform slip, whereas a lower-velocity solution to (20), if any exist, that violates the inequality (21) is unstable.

It seems plausible that if there is very little velocity weakening at this characteristic slip rate V_{dyna}, then the rupture should behave like for a fault with friction that is independent of velocity (e.g., like classical slip-weakening models) and therefore give a cracklike mode of rupture. This expectation is well supported by our numerical simulations, to be discussed. It therefore suggests use of the dimensionless measure

$$T = \{[-d\tau_{ss}(V)/dV]_{V=V_{dyna}}\}/(\mu/2c) \tag{22}$$

of the effective velocity weakening that remains active at the characteristic speed V_{dyna} (which speed is defined when $\tau_0^b > \tau_{pulse}$ and depends on the level of τ_0^b).

This single parameter T does nicely correlate the results of our simulations for $\tau_0^b > \tau_{pulse}$. As will be seen, they show that when τ_0^b is only slightly larger than τ_{pulse}, so that T is near 1 (note that $T = 1$ when $\tau_0^b = \tau_{pulse}$), the rupture mode is always found to be of the self-healing type. On the other hand, when τ_0^b is significantly enough greater than τ_{pulse} that

T is near to zero, we find the expected cracklike rupture mode. Between these extreme values of T, there must be a transition. It is not found to be a sharp one, but, for the 2D cases we have examined, that transition from self-healing to cracklike rupture is found for T in the vicinity of 0.5. Lower values of T around 0.2 to 0.3, that is, higher values of τ_0^b, seem to be needed for transition in 3D simulations (Cochard and Rice, 1997b).

Our results therefore lead us to associate the self-healing rupture mode with low background stresses, $\tau_0^b < \tau_{\text{pulse}}$, or possibly a little greater, $\tau_0^b > \tau_{\text{pulse}}$, but such that T is still not too much less than unity. The crack mode is associated with high stresses, τ_0^b, sufficiently large compared to τ_{pulse} that T is small.

Velocity-Weakening Friction Laws Used in Simulations

The laws we use are adaptations of the Dieterich–Ruina slowness or ageing law (Dieterich, 1979, 1981, 1992; Ruina, 1983), which is expressed as

$$\tau_{\text{strength}} = \tau^* + A \ln(V/\bar{V}_0) + B \ln(\bar{V}_0\theta/L), \qquad d\theta/dt = 1 - V\theta/L. \tag{23}$$

Here, τ^*, A, B, $\bar{V}_0$, and L are constants (the first three proportional to normal stress, assumed constant). The law must be regularized near $V = 0$ for some applications, as done in different ways by Perrin *et al.* (1995) and by Rice (1993) and Rice and Ben-Zion (1996). The latter understand the ln V to originate from an Arrhenius activated rate process when only forward jumps are considered and regularize near $V = 0$ by considering both backward and forward jumps. [Such amounts, essentially, to rewriting the first of equations (23) in the form $V = g(\theta)\exp(\tau_{\text{strength}}/A)$ and then replacing $\exp(\tau_{\text{strength}}/A)$ by $2\sinh(\tau_{\text{strength}}/A)$, which is of no consequence in the normal range for which $\tau_{\text{strength}} \gg A$. We can, further, allow negative V by this procedure when, also, V in the equation for $d\theta/dt$ is replaced by $|V|$.] The law of equation (23) approximately represents data over typical slip rates from 10^{-10} to 10^{-3} m/sec (Dieterich, 1981; Ruina, 1983; Kilgore *et al.*, 1993), as are important for nucleation. It is not known at present how to suitably generalize it for the much higher rates of spontaneous ruptures. We now consider two alternatives.

Perrin-Rice-Zheng (PRZ) Law

Perrin *et al.* (1995) proposed a modified version for the study of ruptures that are suddenly nucleated by overstressing or for which nucleation is not considered but only propagation. This PRZ law retains the ability to restrengthen after rupture is arrested and introduces two cutoff velocity parameters V_0 and V_0/ε:

$$\tau_{\text{strength}} = \tau' + A \ln\left[\frac{V_0 + V}{V_0/\varepsilon + V}\right] + B \ln\left[1 + \theta\frac{V_0(1-\varepsilon)}{\varepsilon L}\right], \qquad \frac{d\theta}{dt} = 1 - \frac{(V_0 + V)\theta}{L}. \tag{24}$$

In (24), V_0 acts as a characteristic speed for velocity weakening, with no weakening at slip rates $V \ll V_0$, and, in this form, $V = 0$ is also allowed. In addition, V_0 gives an upper limit to a contact-time-like state variable $\theta \leqq L/V_0$, and there is an upper limit speed V_0/ε above which there is essentially no further velocity dependence, where $\varepsilon \ll 1$.

At the steady state, that is, $d\theta/dt = 0$, the fault strength is

$$\tau_{ss}(V) = \tau^* + (A - B) \ln\left[\frac{1 + V/V_0}{1 + \varepsilon V/V_0}\right], \tag{25}$$

where $\tau^* = \tau_{\text{upper}} = \tau' + (B - A)\ln(1/\varepsilon)$. We plot $\tau_{ss}(V)/\tau^*$ in Figure 4 for $B/\tau^* = 0.038$, $\varepsilon = 0.001$, for various A/B and V_0. We see that the total strength drop is only a small fraction of τ^* for $A/B = 0.2$. We can make B/τ^* much larger and thus have much greater strength drop, but, in the end, B

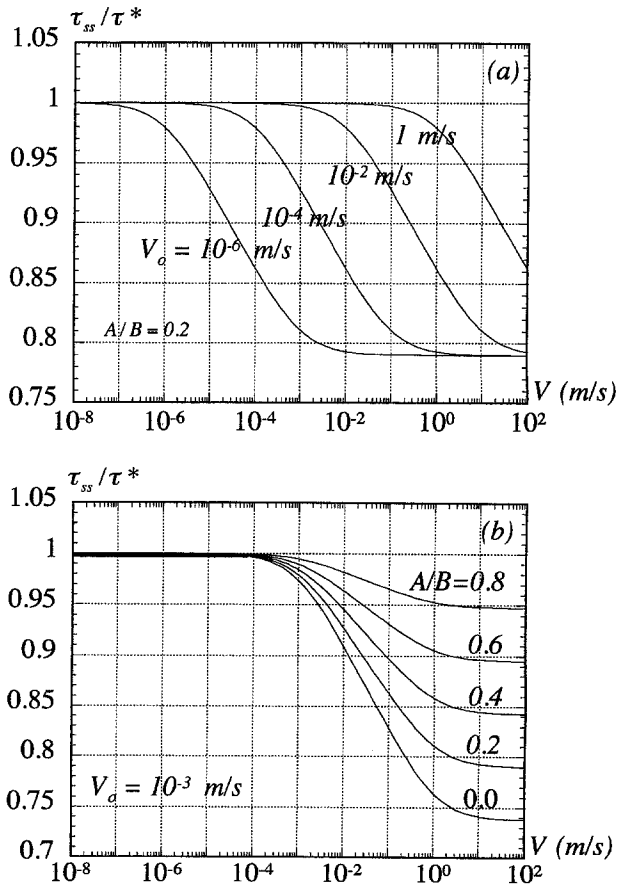

Figure 4. Steady-state strength for the PRZ law with $B/\tau^* = 0.038$, $\varepsilon = 0.001$: (a) $A/B = 0.2$ and various V_0; (b) $V_0 = 10^{-3}$ m/s and various A/B.

can be normalized out of the results to the extent that (for given B/A and ε) results depend only on the dimensionless $\mu V_0/Bc$. Also, the velocity weakening occurs in a way that is evident on the logarithmic scale over a quite broad range of slip rate. For the curve with $V_0 = 10^{-3}$ m/s, weakening occurs from $V = 10^{-4}$ to 1 m/sec.

The law in (24) can be made to coincide approximately with the logarithmic law like in (23) often used to represent laboratory friction data, but, in such case, the cutoff V_0 for the velocity-weakening range should be chosen much smaller than any laboratory rate for which the logarithmic law applies, say, $V_0 = 10^{-10}$ m/sec or less to judge from the granite data of Kilgore *et al.* (1993). Also, to extend such logarithmic law to speeds as high as, say, 1 mm/sec, we must make ε sufficiently small (10^{-7} or less) so that $V_0/\varepsilon = 1$ mm/sec. Also A/τ^* and B/τ^* should then be associated with the small quantities typically denoted a and b [e.g., in Rice (1993)], at least when divided by the friction coefficient f^* corresponding to τ^*. The strength is, however, then essentially a constant at typical slip rates during seismic events, and such seems to allow only cracklike rupture modes on a uniform fault without barriers, as seen by Okubo (1989) and Rice and Ben-Zion (1996).

Thus, to address the way that velocity weakening at higher speeds than the normal laboratory range (i.e., higher than 1 mm/sec or so) may promote self-healing pulses, we use (24) in the spirit of Perrin *et al.* (1995), with V_0 simply being a parameter to mark a representative onset speed for some additional velocity weakening at the higher rates. When we use the law in that way, with V_0 larger than the typical laboratory range, the strength is velocity independent at the very small (compared to V_0) slip rates of the laboratory range. Thus, we cannot use (24) with such V_0 to address nucleation of instability [indeed, we find that the fault surface slips stably, as expected, when we use such law in fault models like that of Rice (1993) or Rice and Ben-Zion (1996), which are driven by an imposed plate rate that is much smaller than V_0]. So, we make use of (24) only for simulations of dynamic rupture in which the details of nucleation under slow load increase are not modeled, and, instead, we nucleate the rupture by overstressing some small region along the fault. The normal expression for nucleation size of Rice (1993), namely, $h^* = 2\mu L/\pi(B - A)$, continues to apply so long as we understand h^* as the critical cell size in the numerical grid to avoid single-cell instabilities when a (several cell) region of fault is slipping near steady state at rates between V_0 and V_0/ε.

For fixed ε and A/B, we may nondimensionalize the velocity by V_0 and stress and strength by B. Then the specifications of (1) and (24) leave a free parameter $\mu V_0/Bc$ on which solutions may depend (see Perrin *et al.*, 1995). That parameter is the ratio of V_0 to a characteristic dynamic slip velocity, cB/μ, in a continuum-sustaining stress reduction of order B. As shown in Figure 4, V_0 and, therefore, the parameter $\mu V_0/Bc$ (we keep cB/μ constant), characterize the weakening behavior of the friction law. So long as ε is made sufficiently small that V_0/ε remains significantly larger than any slip rate experienced during the dynamic rupture, then ε becomes an irrelevant variable, and the only remaining parameters controlling the dynamics and rupture mode, in addition to $\mu V_0/Bc$, are A/B and some suitable nondimensional measure of the remote loading τ_0^b.

Enhanced Velocity-Weakening Law

Here the approach is to develop enhanced velocity-weakening laws that incorporate the Dieterich and Ruina logarithmic representation of the rock friction experimental data like in (23) at low slip rates of the normal laboratory range but also allow the possibility of some significantly enhanced weakening at higher rates. Frictional weakness is reported by Prakash and Clifton (1992, 1993) at slip rates of order 5 to 30 m/sec in their experiments on oblique shock impact of hard metals against cutting tools, and Frutschy and Clifton (1997) point out that continuing weakening is demonstrated over the slip rate ranges of some such experiments. Also, Tsutsumi and Shimamoto (1997), in high rotary slip experiments on gabbro at low normal stress (1.5 MPa), show the onset of pronounced velocity weakening at slip rates of order 1 m/sec, both in situations with and without formation of a melt layer.

We start by recasting the Dieterich–Ruina law of (23) in an approximately equivalent quotient form. Recalling that A/τ^* and B/τ^* are of order 0.01 to 0.04 in the experimental range, with slip rates $V = 10^{-3}$ to $10^3\bar{V}_0$ for $\bar{V}_0 = 1$ μm/sec, the law of (23) is essentially indistinguishable from

$$\tau_{\text{strength}} = \tau^* \frac{1 + (A/\tau^*)\ln(V/\bar{V}_0)}{1 + (B/\tau^*)\ln(L/\bar{V}_0\theta)}, \quad \frac{d\theta}{dt} = 1 - \frac{V\theta}{L}. \tag{26}$$

Again, the $\ln(V/\bar{V}_0)$ can be regularized near $V = 0$ as discussed earlier. In principle, θ (which is essentially an average lifetime of contacting frictional asperities along the fault) can become so large that the denominator approaches zero and then turns negative. For realistic B/τ^*, such happens only for θ of order many tens of thousands to millions of years and does not concern us here. (The effect could be dealt with, if need be, by simply truncating the dependence on θ when, say, τ_{strength} for $V = \bar{V}_0$ reaches the strength of unfaulted rock.) Our concern here is, instead, with inadequacies of (26) at the sorts of θ values occurring during dynamic rupture, which may be 2 to 10 orders of magnitude smaller than θ values in typical laboratory tests over the range previously noted.

If we choose $A = 0.015(\sigma_n - p)$ and $B = 0.019(\sigma_n - p)$, $\tau^* = 0.6(\sigma_n - p)$, with $\sigma_n - p$ being the effective normal stress, then $\tau_{ss}(1.0 \text{ m/sec}) = 0.94\tau_{ss}(1.0 \times 10^{-6} \text{ m/sec})$, which means that τ_{ss} decays very slowly with velocity. Such a slow weakening implies high stress on the fault during slip and, in turn, a high heating rate due to friction. We allow for significantly enhanced high-speed weakening, compared to (26), by rewriting it in the form

$$\tau_{\text{strength}} = \tau^* \frac{1 + (A/\tau^*)\ln(V/\bar{V}_0)}{1 + (B/\tau^*)\ln(L/\bar{V}_0\theta) + H(\theta)}, \quad (27)$$

where $H(\theta)$ is significant only at the very short contact times during rapid slip. We retain the same expression for $d\theta/dt$. A particular choice we explore is

$$H(\theta) = L/V_{\text{weak}}\theta \quad (28)$$

where the new parameter V_{weak} is chosen $\gg 1 \times 10^{-3}$ m/sec to assure agreement with the Dieterich–Ruina law for the laboratory θ range. Then the steady-state strength is

$$\tau_{ss}(V) = \tau^* \frac{1 + (A/\tau^*)\ln(V/\bar{V}_0)}{1 + (B/\tau^*)\ln(V/\bar{V}_0) + V/V_{\text{weak}}}. \quad (29)$$

This implies a direct enhanced weakening effect parameterized by V_{weak} (Fig. 5). In fact, because the logarithmic term becomes essentially independent of V at large V, this weakens like $1/(1 + V/\text{constant})$, a form employed in various earlier studies (Carlson and Langer, 1989; Cochard and Madariaga, 1994). Note that the linear plot, in particular, in Figure 5 can be deceiving; that is a plot of steady-state strength, and some slip displacement (for state evolution) must be undergone to actually realize what is depicted as a very abrupt drop of strength near $V = 0$.

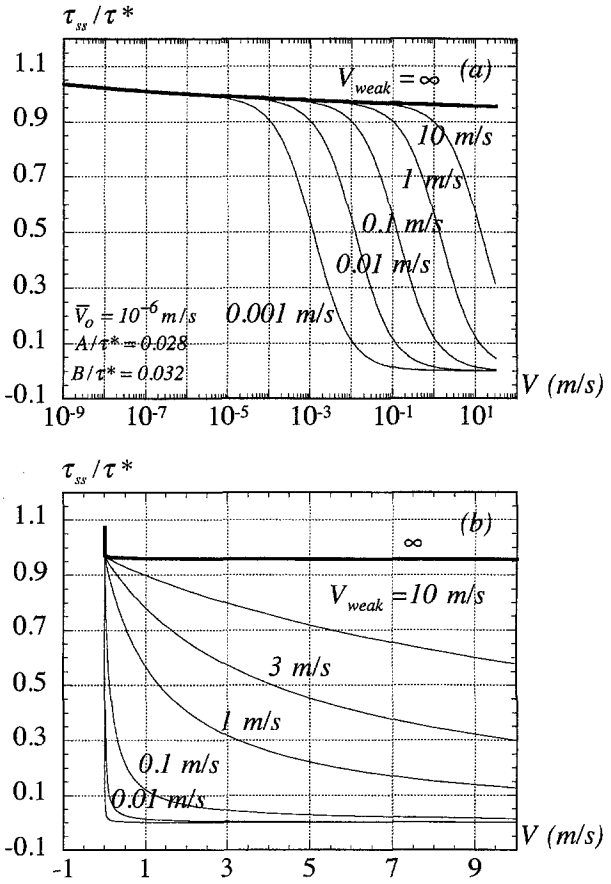

Figure 5. Steady-state strength for the enhanced velocity-weakening law with $\bar{V}_0 = 10^{-6}$ m/sec and various V_{weak}, shown respectively on (a) a logarithmic scale and (b) linear scale for velocity.

Discretization Considerations

We need a guideline for proper numerical discretization of the governing continuous equations. A key parameter to address those issues is the critical spring stiffness for stable steady sliding, as determined for a broad class of rate and state laws by Ruina (1983) and Rice and Ruina (1983).

Related to that is the critical size of a fault segment, corresponding to stiffness μ/segment size, and the critical cell size of a numerical grid such that single-cell instability is precluded and unstable slip episodes involve the cooperative, coherent motion of groups of cells. Rice (1993) denoted the former by h^*; it also can be regarded as a nucleation size, which he called it, or as a coherent slip patch size (Rice and Ben-Zion, 1996). For a one-state-variable law of the rate and state class, with velocity weakening, and for the cellular basis set (i.e., segments of locally uniform slip), Rice (1993) obtained

$$h^* = -\frac{2}{\pi}\frac{\mu}{V(d\tau_{ss}/dV)}L. \quad (30)$$

For the Dieterich–Ruina law of (23), $-V(d\tau_{ss}/dV) \equiv B - A$ is independent of the velocity at which h^* is evaluated. Then we have

$$h^*_{B-A} = \frac{2}{\pi}\frac{\mu}{B - A}L. \quad (31)$$

However, outside the central velocity range of the PRZ law of (24) or at high slip rates in the enhanced velocity-weakening law of (27), the quantity $-V(d\tau_{ss}/dV)$ is a function of velocity. This dependency is important in properly modeling the dynamics of rupture with those laws, because it reflects the weakening behavior at various velocities. Rather than using a varying parameter h^* that differs for different velocities, it is convenient if one h^* can be chosen and the simple h^*_{B-A} is not sufficient. Given the discussion on the dynamics of a uniformly slipping fault in a previous section, a candidate that can act as the representative velocity is V_{dyna}, at least in cases for which it is defined (Fig. 3b). Then (22) and (30) lead us to

$$h^*_{\text{dyna}} = \frac{2}{\pi}\frac{\mu}{[-V(d\tau_{ss}/dV)]|_{V=V_{\text{dyna}}}}L = \frac{4}{\pi}\frac{cL}{V_{\text{dyna}}T}. \quad (32)$$

This makes sense only when $\tau_0^b > \tau_{\text{pulse}}$, so that T is defined, and we have no good alternative in other cases. We want h^* at rapid slip rates to be large compared to cell size h, which condition we can meet approximately, when T is defined, by making h^*_{dyna} of order 10 to 100 cell sizes, although in some cases, as will be seen, even this is not stringent enough. The

problem of accurate numerical discretization is exacerbated by the tendency of the zone near the rupture tip, over which there is rapid state evolution, to contract significantly as the rupture speed approaches the limiting speed (c for antiplane strain). This is analogous to the contraction, at high speeds, of the near-tip breakdown zone in slip-weakening descriptions of dynamic rupture (Rice, 1980).

Examples with PRZ Law

For the PRZ law, the upper bound of the fault strength is $\tau_{\text{upper}} \equiv \tau_{ss}(0) = \tau^*$, and the lower bound is $\tau_{\text{lower}} \equiv \tau_{ss}(\infty) = \tau^* - (B - A)\ln(1/\varepsilon)$. Then the maximum stress change is $\Delta\tau = \tau_{\text{upper}} - \tau_{\text{lower}} = (B - A)\ln(1/\varepsilon)$. It follows that a good way to nondimensionalize the stress in this problem is $\bar{\tau}(x, t) = \tau(x, t) - \tau_{\text{lower}}/\Delta\tau$, which leads to a dimensionless strength threshold $\bar{\tau}_{\text{upper}} = 1.0$. In this section and the next one, we use nondimensional notations to describe the previously defined stress variables. The slip is nondimensionalized as $\bar{\delta} = \delta/L$, where L is the characteristic length of our constitutive law.

The radiation damping line and the steady-state strength can be rewritten as

$$\bar{\tau}_{\text{damp}}(V) = \bar{\tau}_0^b - \frac{\mu V_0/Bc}{2(1 - A/B)\ln(1/\varepsilon)} \frac{V}{V_0}, \qquad (33)$$

$$\bar{\tau}_{ss}(V) = 1 - \frac{1}{\ln(1/\varepsilon)} \ln\left(\frac{1 + V/V_0}{1 + \varepsilon V/V_0}\right),$$

where $\bar{\tau}_0 = \bar{\tau}_0^b$ except within a small region that is overstressed to nucleate the rupture. So if parameters A/B and $\bar{\tau}_0^b$ are further specified, only $\mu V_0/Bc$, which controls the weakening behavior, is left as a parameter to be varied.

We discuss results for a fault consisting of $N_{\text{ele}} = 2048$ elements, replicated periodically with repeat length $\lambda = 2048h$, where h is the length of one element. We also choose a constitutive parameter $\varepsilon = 0.001$. The fault is everywhere in the initial state $\theta = L/V_0$, as it would be after a long time at rest. The uniformly applied stress $\bar{\tau}_0^b$, slightly below the static strength threshold $\bar{\tau}_{\text{upper}}$, acts for $t < 0$ on the fault segment. We also keep stress much lower outside a segment of that repeat length λ (Fig. 1) so that the borders of the segment act as barriers to rupture, allowing us to study the arrest process. We do not address the arrest results here, but they are shown (together with many more examples than we are able to present here) in the Ph.D. thesis by Zheng (1997).

We now illustrate results for two different values of A/B, each at different $\bar{\tau}_0^b$, for a wide range of values of $\mu V_0/Bc$. The higher values of $\mu V_0/Bc$ are such that the background loading corresponds to $\bar{\tau}_0^b < \bar{\tau}_{\text{pulse}}$, whereas the lower values of $\mu V_0/Bc$ cause $\bar{\tau}_0^b > \bar{\tau}_{\text{pulse}}$ and hence should allow the possibility of a cracklike solution. In fact, the range of $\mu V_0/Bc$ considered is chosen to fully illustrate the transition from self-healing to cracklike mode. The value of $\mu V_0/Bc$ at transition will be seen to differ by an order of magnitude between the two cases, but when analyzed in terms of our parameter T, the transition will be seen to take place at roughly the same T value, around 0.5. These two cases are chosen at the extremes of a fuller set of cases presented by Zheng (1997).

Case 1: $A/B = 0.2$ and $\bar{\tau}_0^b = 0.977$

We show the slip histories in this first case with $A/B = 0.2$, and background loading $\bar{\tau}_0^b = 0.977$. Here, $\Delta\tau = 5.526B$ and $\tau_0^b = \tau_{\text{upper}} - 0.126B$. This loading $\bar{\tau}_0^b$ is very close to the strength threshold, being 0.023 smaller. The perturbation $\bar{\tau}_0^p$ is chosen to be nonzero (0.362) over a small portion [size $80h$, or $3.3h^*_{B-A}$, where $\tau_0^p(x, t \geqq 0) = 2.0B$ locally] within the fault segment and brings the total stress $\bar{\tau}_0(x, t)$ to 1.362 in the nucleation portion.

The constitutive laws and radiation damping line are plotted in Figure 6 for $\mu V_0/Bc = 4.0$, 2.0, 1.0, 0.5, and 0.1. The parameter T is shown in Figure 7; it is not defined, so that the understressing condition is satisfied, if $\mu V_0/Bc > 0.86$. Figure 7 shows that T increases smoothly from 0.0 to 1.0, as $\mu V_0/Bc$ goes from 0.0 to 0.86. In comparison, in the next case, we see that for the same range of T increase, $\mu V_0/Bc$ goes from 0.0 to 0.07.

The resulting rupture patterns are shown in Figure 8. Upon decreasing $\mu V_0/Bc$ from 4.0, we find, respectively, a self-healing pulse with nearly uniform but gradually diminishing amount of slip, self-healing pulses with growing slip, then a transitional rupture, and finally a cracklike rupture. The transition occurs around $\mu V_0/Bc = 0.5$ in this case; ruptures propagate in a classical cracklike mode for $\mu V_0/Bc < 0.5$ and in a self-healing mode for $\mu V_0/Bc > 0.5$. The parameter T is not defined for cases $\mu V_0/Bc = 4.0$, 2.0, and 1.0, all larger than 0.86. We have $T = 0.49$ for the transition case with $\mu V_0/Bc = 0.5$, and $T = 0.23$ for the cracklike case shown with $\mu V_0/Bc = 0.1$.

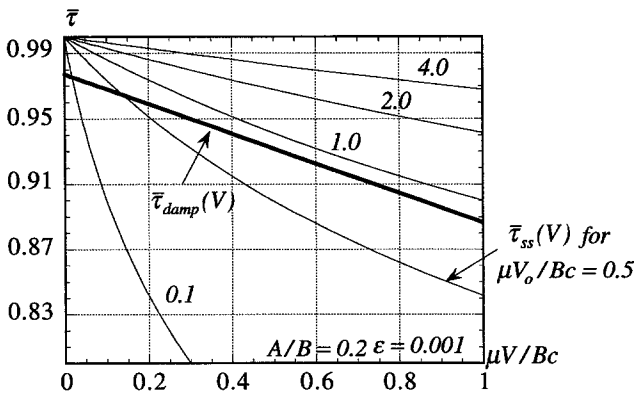

Figure 6. Relative position of the radiation damping line $\bar{\tau}_{\text{damp}}(V)$ to the steady-state strength $\bar{\tau}_{ss}(V)$ for the PRZ law with $\mu V_0/Bc = 4.0$, 2.0, 1.0, 0.5, and 0.1, respectively, with $A/B = 0.2$ and $\bar{\tau}_0^b = 0.977$. T is not defined when $\mu V_0/Bc > 0.86$, which describes a certain range of understressing that is met by the first three cases.

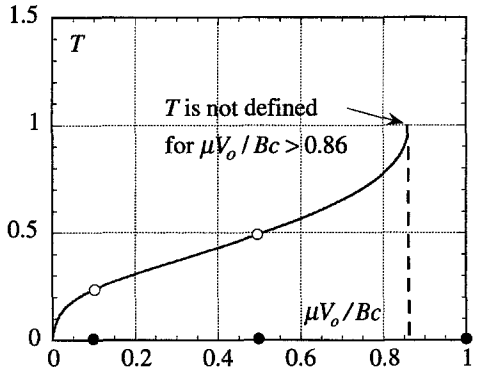

Figure 7. Effects of velocity weakening, which is regulated by parameter $\mu V_0/Bc$, on the parameter T are shown for the PRZ law with $A/B = 0.2$ and $\bar{\tau}_0^b = 0.977$. Dots show some of the cases simulated; T is not defined when $\mu V_0/Bc > 0.86$, the range for which the fault is understressed.

Case 2: $A/B = 0.8$ and $\bar{\tau}_0^b = 0.868$

For this case, $A/B = 0.8$, and we have $\Delta\tau = 1.382B$. The uniform stressing is set to $\bar{\tau}_0^b = 0.868$ in the fault segment, and the ruptures are nucleated by overstressing [$\bar{\tau}_0^p(x, t \geqq 0) = 1.81$, i.e., $\tau_0^p = 2.5B$ locally] over the nucleation portion (of size $160h$ or 5 h_{B-A}^*, where we used $h_{B-A}^* = 32h$). Given the reduction of the maximum stress drop (from $5.526B$ to $1.382B$ for fixed B), which serves as an upper bound of possible weakening, we found the pulselike ruptures are more difficult to nucleate, and a larger stress perturbation $\bar{\tau}_0^p(x, t \geqq 0)$ had to be used.

We plot the relative positions of the constitutive laws to the radiation damping line in Figure 9 for $\mu V_0/Bc = 0.5$, 0.2, 0.1, 0.05, and 0.01. The variation of T, when it is defined, is shown in Figure 10, and, as noted, T increases from 0 to 1 over an order of magnitude smaller range of $\mu V_0/Bc$ compared to the previous case.

The understressing condition is met for $\mu V_0/Bc > 0.071$, and T is not defined then. This is quite different from the 0.86 found with $A/B = 0.2$. As seen in Figure 11, for the given loading $\bar{\tau}_0^b = 0.868$, the slip pulse is quickly arrested for the relatively large $\mu V_0/Bc = 0.5$ but is arrested much more slowly for a smaller $\mu V_0/Bc = 0.2$, and a self-healing pulse of growing slip is found for the case with $\mu V_0/Bc = 0.1$. All those pulses, arrested or not, are associated with $\bar{\tau}_0^b < \bar{\tau}_{\text{pulse}}$. The transition is expected to occur around $T = 0.5$, and it does occur then, corresponding to $\mu V_0/Bc = 0.05$, a value that is a factor of 10 smaller than what we have found for the previous case. A rupture of cracklike mode results for the even smaller $\mu V_0/Bc = 0.01$, which corresponds to $T = 0.21$. So the transition from the cracklike mode to the self-healing mode is consistent with the variation of T and the understressing theory. We see that the parameter T works very well and can be effectively used to predict the slip patterns for $\bar{\tau}_0^b > \bar{\tau}_{\text{pulse}}$.

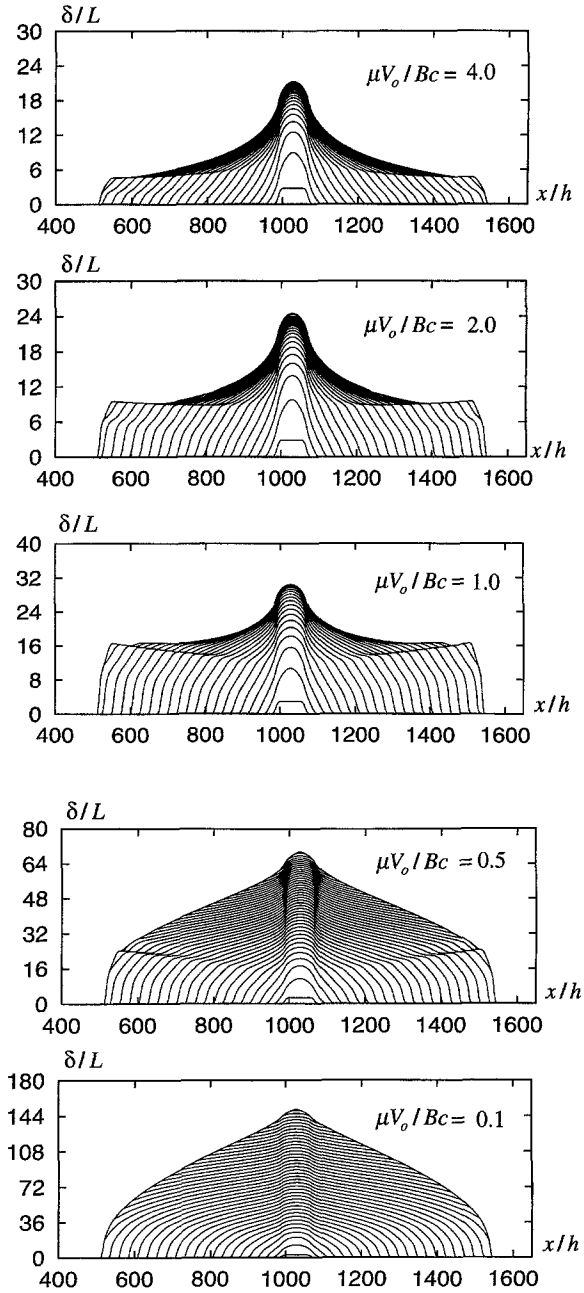

Figure 8. Slip histories for the transient response of a fault under a uniform applied stress $\bar{\tau}_b^0 = 0.977$ with a small portion in the middle locally overstressed. The PRZ law is used with $A/B = 0.2$ and $\varepsilon = 0.001$, and respectively $\mu V_0/Bc = 4.0$, 2.0, 1.0, 0.5, and 0.1. Curves are separated by uniform time increments of 25 h/c Rupture modes are the self-healing pulse for the first three cases from top where the understressing condition is met ($\mu V_0/Bc > 0.86$), while we have the transitional situation with $T = 0.49$ for $\mu V_0/Bc = 0.5$ and cracklike mode with $T = 0.23$ for $\mu V_0/Bc = 0.1$.

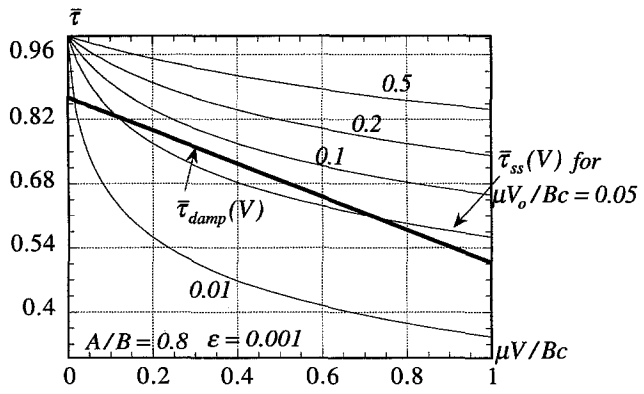

Figure 9. Relative position of the radiation damping line $\bar{\tau}_{damp}(V)$ to the steady-state strength $\bar{\tau}_{ss}(V)$ for $\mu V_0/Bc$ = 0.5, 0.2, 0.1, 0.05, and 0.01, respectively, with A/B = 0.8 and $\bar{\tau}_0^b$ = 0.868. T is not defined when $\mu V_0/Bc > 0.071$, which describes a certain range of understressing and is met by the first three cases.

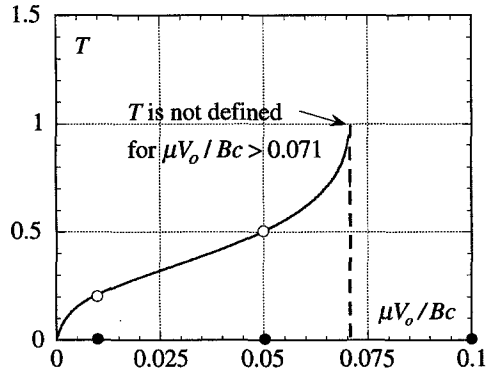

Figure 10. Effects of velocity weakening, regulated by parameter $\mu V_0/Bc$, on T are shown for the PRZ law with A/B = 0.8 and $\bar{\tau}_0^b$ = 0.868. Dots show some of the cases simulated; T is not defined, and the fault is understressed, when $\mu V_0/Bc > 0.071$, a much smaller value than the case with A/B = 0.2 in Figures 6 to 8.

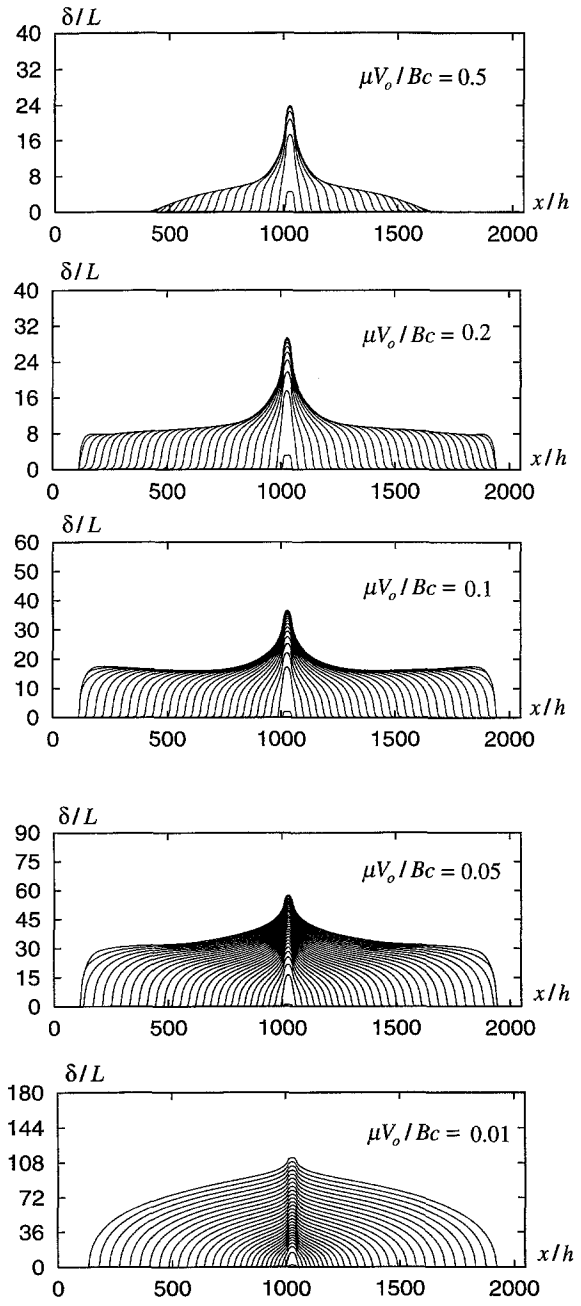

Figure 11. Same as Figure 8 except $\bar{\tau}_b^0$ = 0.868 and A/B = 0.8, and respectively $\mu V_0/Bc$ = 0.5, 0.2, 0.1, 0.05, and 0.01. Rupture modes are the self-healing pulse for the first three cases from top, for which the understressing condition is met ($\mu V_0/Bc > 0.071$), while we have the transitional situation with T = 0.51 for $\mu V_0/Bc$ = 0.05 and the cracklike mode with T = 0.21 for $\mu V_0/Bc$ = 0.01.

Summary for PRZ Law

Elastodynamic modeling results are consistent with the theory developed earlier. The rupture mode is the self-healing one for all the cases satisfying $\bar{\tau}_0^b < \bar{\tau}_{pulse}$, a condition under which the fault is so understressed that the whole radiation damping line lies below the steady-state strength curve. The parameter T is not defined in this loading range, as depicted in plots of T versus $\mu V_0/Bc$ for the different $\bar{\tau}_0^b$ and A/B.

We summarize the results given here and of other cases presented in the thesis by Zheng (1997) in Table 1, where for various combinations of $\bar{\tau}_0^b$ and A/B, there are indicated a set of values of $\mu V_0/Bc$ for which the response is definitely cracklike, another set (all which happen to coincide with conditions for which $\bar{\tau}_0^b < \bar{\tau}_{pulse}$) for which the response is in the self-healing mode and an intermediate set corresponding to transition. The transition is not sharply defined. Our cases 1 and 2 correspond, respectively, to the rightmost and leftmost columns in the table. The same set is shown in Table 2, where the corresponding T values are given in the situations for which $\bar{\tau}_0^b > \bar{\tau}_{pulse}$ so that T is defined. All of the T values at transition are indeed seen to be in the vicinity of

0.5, although, again, we emphasize that the transition is not sharply defined. The best summary of results might be to say that it occurs for T between, approximately, 0.4 and 0.6, and that the cracklike mode occurs for T below approximately 0.3.

Inspection of Figures 8 and 11 shows that the amount of slip is far greater when rupture is by the cracklike mode than by the self-healing mode.

Examples with Enhanced Velocity-Weakening Law

We generally keep the notations the same as those in the previous section. The lower stress bound is zero because of the extra weakening, that is, $\tau_{\text{lower}} \equiv \tau_{ss}(\infty) = 0.0$. The upper bound, however, cannot be chosen simply as $\tau_{ss}(0)$ because the law is not regularized at $V = 0$. A good substitute is $\tau_{\text{upper}} = \tau^* = f_0 \times (\sigma_n - p)$, where f_0 is chosen as 0.5 to 0.6, and $\sigma_n - p$ is the effective normal stress. The stress drop is then $\Delta\tau = \tau_{\text{upper}} - \tau_{\text{lower}} = \tau^*$, and the stress is nondimensionalized as

$$\bar{\tau}(x, t) = \frac{\tau(x, t) - \tau_{\text{lower}}}{\Delta\tau} = \frac{\tau(x, t)}{\tau^*}.$$

Again we have the nondimensionalized slip $\bar{\delta} = \delta/L$.

The nondimensionalized version of the radiation damping line and the steady-state strength are

$$\bar{\tau}_{\text{damp}}(V) = \bar{\tau}_0 - \frac{\mu\bar{V}_0}{2\tau^* c}\frac{V}{\bar{V}_0}, \quad \bar{\tau}_{ss}(V) = \frac{1 + (A/\tau^*)\ln(V/\bar{V}_0)}{1 + (B/\tau^*)\ln(V/\bar{V}_0) + (V/\bar{V}_0)/(V_{\text{weak}}/\bar{V}_0)}, \tag{34}$$

Table 1
Range of $\mu V_0/Bc$ under Various Weakening and Loading Conditions

	$A/B = 0.8$		$A/B = 0.2$	
	$\bar{\tau}_0^b = 0.868$	$\bar{\tau}_0^b = 0.977$	$\bar{\tau}_0^b = 0.868$	$\bar{\tau}_0^b = 0.977$
Crack	0.01	0.01	0.1	0.1
Transition	0.05	0.12	0.23	0.5
Pulse	0.1	0.3	0.5	1.0

Table 2
Values of T under Various Weakening and Loading Conditions

	$A/B = 0.8$		$A/B = 0.2$	
	$\bar{\tau}_0^b = 0.868$	$\bar{\tau}_0^b = 0.977$	$\bar{\tau}_0^b = 0.868$	$\bar{\tau}_0^b = 0.977$
Crack	0.21	0.17	0.32	0.23
Transition	0.51	0.48	0.59	0.49
Pulse*	$\bar{\tau}_0^b < \bar{\tau}_{\text{pulse}}$	$\bar{\tau}_0^b < \bar{\tau}_{\text{pulse}}$	$\bar{\tau}_0^b < \bar{\tau}_{\text{pulse}}$	$\bar{\tau}_0^b < \bar{\tau}_{\text{pulse}}$

*$\bar{\tau}_0^b < \bar{\tau}_{\text{pulse}}$ implies understressing and no definition of T.

where again $\bar{\tau}_0 = \bar{\tau}_0^b$ except within a very small region that is overstressed to nucleate the rupture.

In the following simulations, the fault starts from the initial state $\theta = L/V_0$. We choose $\bar{V}_0 = 1.0 \times 10^{-6}$ m/sec, $A = 0.014(\sigma_n - p)$, $B = 0.016(\sigma_n - p)$, and $\tau^* = 0.5(\sigma_n - p)$. The effective normal stress $\sigma_n - p$ is chosen as 200 bars, which results in a stress drop $\Delta\tau = 100$ bars. So the only parameters left to be determined are V_{weak} and $\bar{\tau}_0^b$. A similar loading configuration is used, but with a longer length of nucleation portion within the highly stressed fault segment. The large nucleation size is required because a very large h^*_{B-A}/h ($=320$) is necessary in our modeling to overcome the discretization effects and, as will be seen, even this becomes marginally suitable outside the self-healing pulse range.

The responses of a fault under various background loadings $\bar{\tau}_0^b$ are investigated for a fixed $V_{\text{weak}} = 3.0$ m/sec. The stressing level $\bar{\tau}_{\text{pulse}}$ is found to be 0.974, and then the radiation damping line has a tangent point with the steady-state strength curve only at $V_{\text{dyna}} = 9.02 \times 10^{-3}$ m/sec. Again, $N_{\text{ele}} = 2048$ elements are used. The perturbed part $\bar{\tau}_0^p$ is nonzero ($=2.912$) only over a portion of 120 elements.

The steady-state constitutive law and radiation damping lines with $\bar{\tau}_0^b = 0.8$, 0.864, 0.928, 0.992, and 1.056 are shown in Figure 12, and the T variation with loading is shown in Figure 13. Five rupture processes are shown, respectively, under the same suddenly imposed $\bar{\tau}_0^p$ at time zero, in Figure 14. We obtained a quickly arresting pulselike rupture process with $\bar{\tau}_0^b = 0.8$, a loading level well below $\bar{\tau}_{\text{pulse}} = 0.974$. Then we have a slowly diminishing pulse with $\bar{\tau}_0^b = 0.864$, and a slowly growing pulse with $\bar{\tau}_0^b = 0.928$. Further increase of loading $\bar{\tau}_0^b$ leads to a rupture process exhibiting what seems to be transitional behavior between the self-healing pulse and the cracklike modes for $\bar{\tau}_0^b = 0.992$, with $T = 0.48$. The response is more cracklike

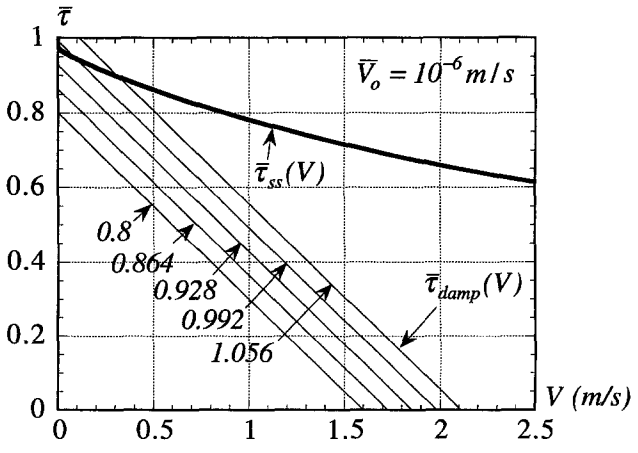

Figure 12. Relative position of the radiation damping line $\bar{\tau}_{\text{damp}}(V)$ to the steady-state strength $\bar{\tau}_{ss}(V)$ for the enhanced velocity-weakening law, for various $\bar{\tau}_0^b$, with $V_{\text{weak}} = 3.0$ m/sec for the enhanced velocity-weakening law. For this case, no intersection can be found if $\bar{\tau}_0^b < \bar{\tau}_{\text{pulse}} = 0.974$.

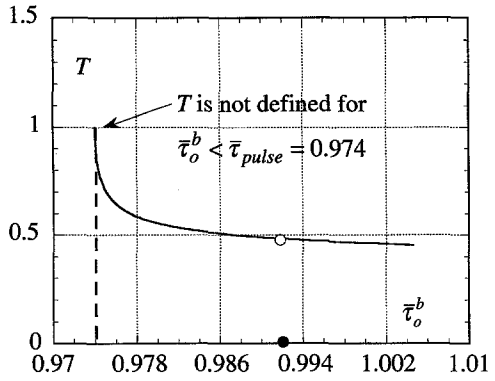

Figure 13. Effects of loading, which is represented by parameter $\bar{\tau}_0^b$, on parameter T are shown for the enhanced velocity-weakening law with V_{weak} = 3.0 m/sec. Dot shows a case simulated; T changes rapidly only within a small range of $\bar{\tau}_0^b$, as shown, and is defined only for $\bar{\tau}_0^b < \bar{\tau}_{pulse} = 0.974$.

for the higher $\bar{\tau}_0^b = 1.056$, with $T = 0.4$, although it is evident that small zones of transient healing still form over short distances near the advancing rupture front [more detailed study of the phenomenon by Nadia Lapusta (private commun., 1998), with much greater refinement of the computational grid than here, suggests that these transient healing zones are real and not a numerical artifact]. Because T decreases very slowly with the increase of $\bar{\tau}_0^b$, we cannot get a pure cracklike mode unless for a case with an extremely large $\bar{\tau}_0^b$. Thus, while we cannot give a suitable numerical treatment of the low T range in this case, the results under conditions leading to self-healing pulses again support the understressing theory given earlier, and transition seems to be underway for T in the vicinity of 0.5.

Simulation of Self-healing Pulses Propagating in Nonuniform Stress Fields

These simulations are done for the PRZ law of equation (24) with $A/B = 0.2$ (like for case 1 earlier) and $\mu V_0/Bc = 0.5$. For such parameters, we can calculate $\bar{\tau}_{upper}$ and $\bar{\tau}_{pulse}$ as before.

We divide the fault into three segments, with each having different loading conditions (Fig. 15). The self-healing slip pulse is nucleated at the left then propagates to the right through those three regions. We observe clearly that the pulse grows in quite different ways under different loading levels. The slip amplitude left behind the traveling slip pulse grows rapidly within the region where loading is closer to the threshold but grows more slowly in regions where loading is further away from the threshold.

Conclusion

We have developed a prescription for understanding the mode of rupture propagation under a uniform background stress τ_0^b on an unbounded fault obeying a velocity-weakening constitutive law with rate and state dependence. At the simplest level, ruptures propagating under high τ_0^b are of the enlarging crack type, and those propagating under low τ_0^b are self-healing pulses.

More precisely, the constitutive law defines a stress level τ_{pulse}, such that if $\tau_{ss}(V)$ is the strength for steady-state sliding at slip rate V, then τ_{pulse} is the largest value of τ_0^b

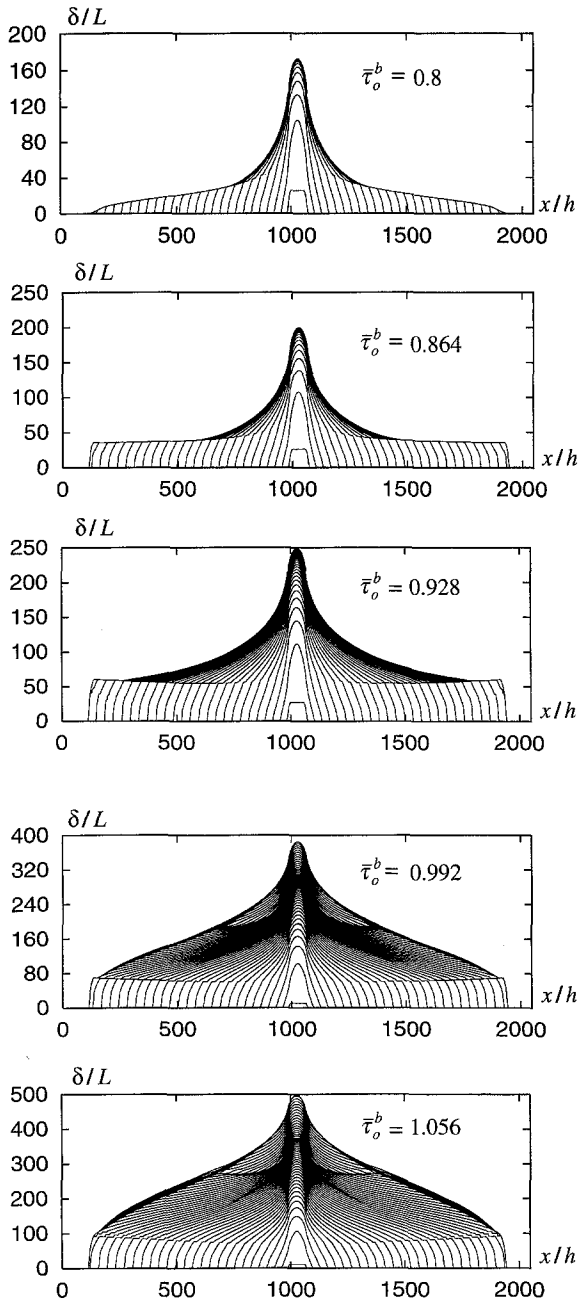

Figure 14. Slip histories for the transient response of a fault under various uniform applied stresses $\bar{\tau}_b^0$ and a small portion in the middle locally overstressed. The enhanced velocity-weakening law is used with V_{weak} = 3.0 m/sec. Rupture modes are the self-healing pulse for the first three cases where the understressing condition is met ($\bar{\tau}_0^b > \bar{\tau}_{pulse} = 0.974$), while we have a transitional situation for higher $\bar{\tau}_0^b$.

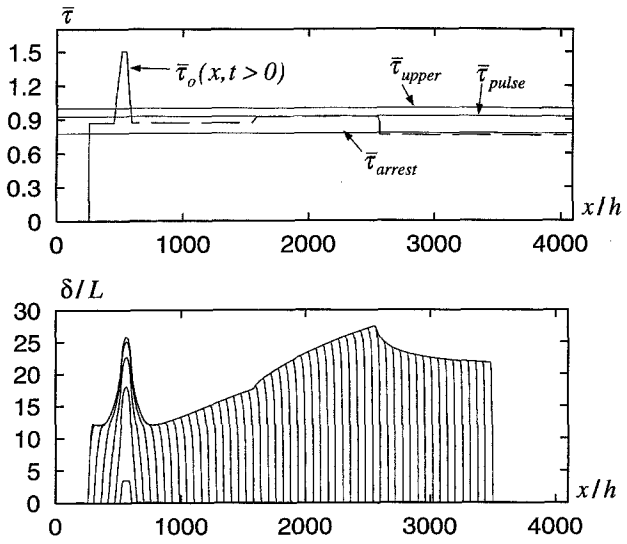

Figure 15. Initial stress and the slip history on the fault for the PRZ law showing effects of loading. We used $A/B = 0.2$ and $\mu V_0/Bc = 0.5$. (a) Background loading is set up to nucleate ruptures at left, and a step increase plus a step decrease define three different local background loading conditions to the right of the nucleation segment. Thin horizontal lines show three reference stressing levels $\bar{\tau}_{upper}$, $\bar{\tau}_{pulse}$, and $\bar{\tau}_{arrest}$, respectively, in the same order from top. (b) Slip history with time interval 30 h/c.

satisfying $\tau_0^b - (\mu/2c)V \leqq \tau_{ss}(V)$ for all $V > 0$. That is, like illustrated in Figure 3, when $\tau_0^b = \tau_{pulse}$, the radiation damping line $\tau = \tau_{pulse} - (\mu/2c)V$, in a τ versus V plot, makes tangential contact with the strength curve $\tau = \tau_{ss}(V)$.

We have proven the theorem that when $\tau_0^b < \tau_{pulse}$, solutions in the form of indefinitely enlarging cracks (i.e., without healing) cannot exist, at least solutions cannot in which the crack increases (or fails to decrease) the shear force borne by the part of the fault lying outside of the rupture zone. Thus, solutions when $\tau_0^b < \tau_{pulse}$ are expected to be of the self-healing pulse type.

Numerical simulations of 2D antiplane rupture, done for two types of rate and state constitutive laws, confirm that. When $\tau_0^b < \tau_{pulse}$, the slip within the pulse may either decrease, remain constant, or increase with rupture propagation distance. In the former case, corresponding to the lowest stress levels, the rupture ultimately arrests. At a particular stress level τ_{arrest}, which is the upper limit to that lowest stress range, the pulse propagates steadily with constant slip; that case was investigated by Perrin *et al.* (1995), who emphasized that such solutions can exist only for laws with state evolution features allowing strength increase with time on the healed (no longer slipping) part of the rupture. All simulations at stress $\tau_0^b = \tau_{pulse}$ show self-healing pulses whose slip amplitude grows with propagation distance. Thus, $\tau_{pulse} > \tau_{arrest}$.

At higher background stresses, $\tau_0^b > \tau_{pulse}$, there is no general theorem to rule out particular types of solutions. We find from the simulations that self-healing pulse solutions exist for stresses that are only slightly above τ_{pulse}, whereas at higher stresses, the mode of rupture is in the form of an enlarging shear crack.

We show that a parameter T can be introduced to characterize these ranges. It is defined whenever $\tau_0^b > \tau_{pulse}$. Then, the equation $\tau_0^b - (\mu/2c)V = \tau_{ss}(V)$ has at least one solution on $V > 0$; we call V_{dyna} the largest such solution (Fig. 3b), which we understand as a characteristic slip velocity of the rupture process. A dimensionless measure of the strength of continuing velocity weakening at that velocity is $T = [-d\tau_{ss}(V)/dV](\mu/2c)$ and, when $\tau_0^b = \tau_{pulse}$, $T = 1$, but T reduces toward zero as τ_0^b is increased above τ_{pulse}. We expect low values of T to correspond to the cracklike rupture mode, because that is the mode when the strength on well-slipped parts of the rupture is insensitive to velocity (like in slip-weakening models).

This is indeed confirmed by our simulations. They show the following in the loading range $\tau_0^b > \tau_{pulse}$: (1) When T is near 1, say $1.0 \geqq T > 0.6$, which means that τ_0^b is only slightly higher than τ_{pulse}, the rupture mode is of self-healing pulse type (with amount of slip growing with distance of rupture propagation). (2) When T is near zero, say $0.4 > T \geqq 0$, which range is achieved by increasing τ_0^b sufficiently above τ_{pulse}, the rupture is in the form of an enlarging shear crack, with no development of a healing zone. The transition from self-healing to cracklike mode occurs in the vicinity of $T \approx 0.5$. Cochard and Rice (1997b) find T to be an equally valid parameter in 3D rupture simulations, but then the transition value is lower, $T = 0.3$, so that higher stresses τ_0^b are required for rupture to be in the enlarging crack mode.

This classification in terms of τ_{pulse}, and of the additional parameter T when $\tau_0^b > \tau_{pulse}$, concisely explains our results for different classes of constitutive laws and for wide ranges of parameter choices within a given class.

Our limited studies of rupture propagation under spatially variable prestress suggest that when rupture is in the self-healing mode, the character of the pulse (whether with growing or decreasing amount of slip) quickly adjusts to the local level of the prestress.

The Gutenberg–Richter frequency versus size statistics of earthquakes tells us that for every 1 earthquake that achieves, say, magnitude 3 size but does not arrest and, rather, grows to magnitude 4, there are approximately 10 that do arrest at that smaller size, and so on for other magnitudes, at least within the range for which there is power-law scaling with $b \approx 1$. An interpretation of such results is to say that faults are chronically understressed, so that most ruptures simply fail to become large. Such understressing is likely to be very heterogeneous and not like the uniform τ_0^b considered here. Nevertheless, if natural faults are indeed velocity weakening at seismic slip rates, so that our present analysis applies, then it is plausible to make the association that these faults are lightly stressed and perhaps understressed in the precise meaning of the term here. In such case, then, we could understand that the self-healing mode of rup-

ture would be a pervasive one, because the stresses are too low on average to allow the cracklike mode and can do so only at places of local stress concentration where rupture nucleates.

We emphasize that this study has been on understanding the rupture mode in the presence of velocity-weakening friction on a fault of spatially uniform properties between identical linear elastic solids. As explained in the Introduction, other mechanisms of self-healing pulse generation exist and involve, for example, strong spatial nonuniformity of frictional weakening properties within the fault zone or dissimilarity of elastic properties across the fault.

Acknowledgments

The studies were supported by the NSF Southern California Earthquake Center through PO# 569928 to Harvard, and by the U.S. Geological Survey through Grants 1434-HQ-96-GR-02735 and 1434-HQ-97-GR-03094. We are grateful to Yehuda Ben-Zion, Alain Cochard, Nadia Lapusta, and John Morrisey for discussions. Further, we are grateful to Alain Cochard for a careful reading of an earlier version of the manuscript and for recalculations, done with assistance of Nadia Lapusta, confirming that a figure of an earlier version of the article [same as Fig. 4-4 of Zheng (1997)] contained a feature that was in error due to periodic wraparound in the spectral formulation.

References

Adams, G. G. (1995). Self-excited oscillations of two elastic half-spaces sliding with a constant coefficient of friction, *J. Appl. Mech.* **62,** 867–872.

Adams, G. G. (1998). Steady sliding of two elastic half-spaces with friction reduction due to interface stick-slip, *J. Appl. Mech.* **65,** 470–475.

Andrews, D. J. (1976a). Rupture propagation with finite stress in antiplane strain, *J. Geophys. Res.* **81,** 3575–3582.

Andrews, D. J. (1976b). Rupture velocity of plane strain shear cracks, *J. Geophys. Res.* **81,** 5679–5687.

Andrews, D. J. (1985). Dynamic plane-strain shear rupture with a slip-weakening friction law calculated by a boundary integral method, *Bull. Seism. Soc. Am.* **75,** 1–21.

Andrews, D. J. and Y. Ben-Zion (1997). Wrinkle-like slip pulse on a fault between different materials, *J. Geophys. Res.* **102,** 553–571.

Beeler, N. M. and T. E. Tullis (1996). Self-healing slip pulse in dynamic rupture models due to velocity-dependent strength, *Bull. Seism. Soc. Am.* **86,** 1130–1148.

Ben-Zion, Y. and J. R. Rice (1997). Dynamic simulations of slip on a smooth fault in an elastic solid, *J. Geophys. Res.* **102,** 17771–17784.

Beroza, G. C. and T. Mikumo (1996). Short slip duration in dynamic rupture in the presence of heterogeneous fault properties, *J. Geophys. Res.* **101,** 22449–22460.

Brune, J. N. (1976). The physics of earthquake strong motion, in *Seismic Risk and Engineering Decisions,* C. Lominitz and E. Rosenblueth (Editors), Elsevier, New York, 141–171.

Carlson, J. M. and J. S. Langer (1989). Mechanical model of an earthquake fault, *Phys. Rev. A* **40,** 6470–6484.

Cochard, A. and R. Madariaga (1994). Dynamic faulting under rate-dependent friction, *Pure Appl. Geophys.* **142,** 419–445.

Cochard, A. and R. Madariaga (1996). Complexity of seismicity due to highly rate dependent friction, *J. Geophys. Res.* **101,** 25321–25336.

Cochard, A. and J. R. Rice (1997a). A spectral method for numerical elastodynamic fracture analysis without spatial replication of the rupture event, *J. Mech. Phys. Solids* **45,** 1393–1418.

Cochard, A. and J. R. Rice (1997b). Mode of rupture, self-healing slip pulse versus enlarging shear crack, for a velocity-weakening fault in a 3D solid (abstract), *EOS* **78,** no. 46 (Fall Meeting Suppl.), F472.

Das, S. (1980). A numerical method for determination of source time functions for general three-dimensional rupture propagation, *Geophys. J. R. Astr. Soc.* **62,** 591–604.

Das, S. and B. V. Kostrov 1987. On the numerical boundary integral method for three-dimensional dynamic shear crack problems, *J. Appl. Mech.* **54,** 99–104.

Day, S. M. (1982). Three-dimensional finite difference simulation of fault dynamics: rectangular faults with fixed rupture velocity, *Bull. Seism. Soc. Am.* **72,** 705–727.

Day, S. M., G. Yu, and D. J. Wald (1998). Dynamic stress changes during earthquake rupture, *Bull. Seism. Soc. Am.* **88,** 512–522.

Dieterich, J. H. (1979). Modeling of rock friction: 1. Experimental results and constitutive equations, *J. Geophys. Res.* **84,** 2161–2168.

Dieterich, J. H. (1981). Constitutive properties of faults with simulated gouge, in *Mechanical Behavior of Crustal Rocks,* N. L. Carter, M. Friedman, J. M. Logan, and D. W. Stearns (Editors), *Geophysical Monograph 24,* American Geophysical Union, Washington, D.C., 103–120.

Dieterich, J. H. (1992). Earthquake nucleation on faults with rate- and state-dependent strength, *Tectonophysics* **211,** 115–134.

Freund, L. B. (1979). The mechanics of dynamic shear crack propagation, *J. Geophys. Res.* **84,** 2199–2209.

Frutschy, K. J. and R. J. Clifton (1997). Plate-impact technique for measuring dynamic friction at high temperatures, *Trans. Am. Soc. Mech. Eng., J. Tribol.* **119,** 590–593.

Fukuyama, E. and R. Madariaga (1998). Rupture dynamics of a planar fault in a 3D elastic medium: rate- and slip-weakening friction, *Bull. Seism. Soc. Am.* **88,** 1–17.

Geubelle, P. H. and J. R. Rice (1995). A spectral method for 3D elastodynamic fracture problems, *J. Mech. Phys. Solids* **43,** 1791–1824.

Harris, R. A. and S. M. Day (1993). Dynamics of fault interaction: parallel strike-slip faults, *J. Geophys. Res.* **98,** 4461–4472.

Harris, R. and S. M. Day (1997). Effect of a low velocity zone on a dynamic rupture, *Bull. Seism. Soc. Am.* **87,** 1267–1280.

Heaton, T. H. (1990). Evidence for and implications of self-healing pulses of slip in earthquake rupture, *Phys. Earth Planet. Interiors* **64,** 1–20.

Ida, Y. (1972). Cohesive force across the tip of a longitudinal-shear crack and Griffith's specific surface energy, *J. Geophys. Res.* **77,** 3796–3805.

Johnson, E. (1990). On the initiation of unidirectional slip, *Geophys. J. Int.* **101,** 125–132.

Johnson, E. (1992). The influence of the lithospheric thickness on bilateral slip, *Geophys. J. Int.* **101,** 151–160.

Kilgore, B. D., M. L. Blanpied, and J. H. Dieterich (1993). Velocity and normal stress dependent friction of granite, *Geophys. Res. Lett.* **20,** 903–906.

Kostrov, B. V. (1966). Unsteady propagation of longitudinal shear cracks, *J. Appl. Math. Mech.* **30,** 1241–1248.

Madariaga, R. (1976). Dynamics of an expanding circular fault, *Bull. Seism. Soc. Am.* **66,** 639–666.

Okubo, P. G. (1989). Dynamic rupture modeling with laboratory-derived constitutive relations, *J. Geophys. Res.* **94,** 12321–12335.

Olsen, K. G., R. Madariaga, and R. J. Archuleta (1997). Three-dimensional dynamic simulation of the 1992 Landers earthquake, *Science* **278,** 834–838.

Palmer, A. C. and J. R. Rice (1973). The growth of slip surfaces in the progressive failure of overconsolidated clay slopes, *Proc. R. Soc. London Ser. A* **332,** 527–548.

Perrin, G., J. R. Rice, and G. Zheng (1995). Self-healing slip pulse on a frictional surface, *J. Mech. Phys. Solids* **43,** 1461–1495.

Prakash, V. and R. J. Clifton (1992). Pressure-shear plate impact measurement of dynamic friction for high speed machining applications, in *Proc. of VII International Congress on Experimental Mechanics, Las Vegas, June 1992,* Society of Experimental Mechanics.

Prakash, V. and R. J. Clifton (1993). Time-resolved dynamic friction mea-

surements in pressure-shear, in *Experimental Techniques in the Dynamics of Deformable Solids,* Appl. Mech. Div., Vol. 165 (AMD-Vol. 165), ASME, New York, 33–48.
Rice, J. R. (1980). The mechanics of earthquake rupture, in *Physics of the Earth's Interior,* A. M. Dziewonski and E. Boschi (Editors), Italian Physical Society / North Holland, Amsterdam, 555–649.
Rice, J. R. (1993). Spatio-temporal complexity of slip on a fault, *J. Geophys. Res.* **98,** 9885–9907.
Rice, J. R. (1997). Slip pulse at low driving stress along a frictional fault between dissimilar media (abstract), *EOS* **78,** no. 46 (Fall Meeting Suppl.), F464.
Rice, J. R. and Y. Ben-Zion (1996). Slip complexity in earthquake fault models, *Proc. Natl. Acad. Sci. USA* **93,** 3811–3818.
Rice, J. R. and A. L. Ruina (1983). Stability of steady frictional slipping, *J. Appl. Mech.* **50,** 343–349.
Rice, J. R. and S. T. Tse (1986). Dynamic motion of a single degree of freedom system following a rate and state dependent friction law, *J. Geophys. Res.* **91,** 521–530.
Ruina, A. L. (1983). Slip instability and state variable friction laws, *J. Geophys. Res.* **88,** 10359–10370.
Tsutsumi, A. and T. Shimamoto (1997). High-velocity frictional properties of gabbro, *Geophys. Res. Lett.* **24,** 699–702.
Weertman, J. (1980). Unstable slippage across a fault that separates elastic media of different elastic constants, *J. Geophys. Res.* **85,** 1455–1461.
Zheng, G. (1997). Dynamics of the earthquake source: an investigation of conditions under which velocity-weakening friction allows a self-healing versus crack-like mode of rupture, *Ph.D. Thesis,* Division of Engineering and Applied Sciences, Harvard University.

Appendix 1

Elastodynamic Functional ϕ for 2D Antiplane Strain

In 2D cases, equation (1) reduces to

$$\tau(x,t) = \tau_0(x,t) + \phi(x,t) - \frac{\mu}{2c} V(x,t). \quad \text{(A1.1)}$$

The functional is given by Cochard and Rice (1997a) as the integral

$$\phi(x,t) = \frac{\mu}{2\pi} \frac{\partial^2}{\partial x^2} \int_0^t \int_{-\infty}^{+\infty} M\left[\frac{x-\xi}{c(t-q)}\right] \frac{\delta(\xi,q)}{t-q}\, d\xi dq, \quad \text{(A1.2)}$$

where they give the function $M[u]$ for antiplane and for in-plane slip (and also for tensile opening). In the antiplane case,

$$M[u] = \begin{cases} \sqrt{1-u^2}, & |u| < 1 \\ 0, & |u| > 1 \end{cases}. \quad \text{(A1.3)}$$

For numerical treatments, we follow the spectral methodology of Perrin *et al.* (1995), representing both slip δ and the functional ϕ as Fourier series that are truncated at some large order,

$$\begin{Bmatrix} \delta(x,t) \\ \phi(x,t) \end{Bmatrix} = \sum_{n=-N/2}^{n=+N/2} \begin{Bmatrix} D(k_n,t) \\ F(k_n,t) \end{Bmatrix} e^{ik_n x}, \quad \text{(A1.4)}$$

where N is even, $k_n = 2\pi n/\lambda$, and λ is a repeat length for the series. Then the Fourier coefficients are related by a convolution that, for the case of antiplane slip, is

$$F(k,t) = -\frac{\mu k}{2} \int_0^t \frac{J_1(kcq)}{q} D(k,t-q)dq. \quad \text{(A1.5)}$$

Further details of the numerical method are discussed by Perrin *et al.* (1995).

Appendix 2

Proof That a 2D Antiplane Rupture Increases or Does Not Decrease the Shear Force Sustained Outside the Ruptured Zone

Assume that a 2D rupture has, at time t, slipped a region occupying $-L(t) < x < +L(t)$, with symmetry of the slip distribution relative to $x = 0$. Because $V = 0$ for $|x| > L(t)$, we have $\tau = \tau_0^b + \phi$ there, and the integral of equation (15) becomes

$$\int_{S_{\text{out}}(t)} [\tau(x,t) - \tau_0^b]dx = 2\int_{L(t)}^{\infty} [\tau(x,t) - \tau_0^b]dx = 2\int_{L(t)}^{\infty} \phi(x,t)dx$$
$$= -\frac{\mu}{\pi}\left\{\frac{\partial}{\partial x}\int_0^t \int_{-\infty}^{+\infty} M\left[\frac{x-\xi}{c(t-q)}\right] \frac{\delta(\xi,q)}{t-q}\, d\xi dq\right\}_{x=L(t}$$
(A2.1)

To further interpret the last expression, we operate on M with $\partial/\partial x$ and then note that because M is homogeneous of degree zero in $(x-\xi)$ and $(t-q)$,

$$(x-\xi)\partial M/\partial x = -(t-q)\partial M/\partial t$$
$$= (t-q)\partial M/\partial q. \quad \text{(A2.2)}$$

Then, so expressing $\partial M/\partial x$ and integrating by parts on q, we get

$$\int_{S_{\text{out}}(t)} [\tau(x,t) - \tau_0^b]dx$$
$$= \frac{\mu}{\pi}\int_0^t \int_{-L(t)}^{L(t)} M\left[\frac{L(t)-\xi}{c(t-q)}\right] \frac{V(\xi,q)}{L(t)-\xi}\, d\xi dq, \quad \text{(A2.3)}$$

where, of course, $V(\xi, q) = \partial\delta(\xi, q)/\partial q$ and we have set $x = L(t)$.

This analysis could apply for in-plane or antiplane slip. In both cases, $V(\xi, q)$ and $L(t) - \xi$ in the integrand are everywhere non-negative. For the antiplane case $M[u]$, given by (A1.3), is likewise non-negative, and hence, it is a definitive result in that case that

$$\int_{S_{\text{out}}(t)} [\tau(x,t) - \tau_0^b]dx \geqq 0, \quad \text{(A2.4)}$$

like assumed in equation (15). The difficulty in generating a similar general proof of (15) for the case of in-plane slip is that $M[u]$ is then not positive for all values of u.

Appendix 3

Stability of Steady-State Solutions under Conditions of Spatially Uniform Slip

We now show that the solution for spatially uniform slip at steady state on a fault obeying the velocity-weakening friction law is stable at a solution like $V = V_{\text{dyna}}$ illustrated in Figure 3, for which the negative of the slope of steady-state strength $\tau_{ss}(V)$ is smaller than the negative of the slope of the radiation damping line $\mu/2c$, and unstable otherwise.

To prove that, we write the rate- and state-dependent friction law as in (6) to (12). Taking the derivative relative to V for both equations (8) and (9), we have

$$\begin{aligned} d\tau_{ss}/dV &= F_V + F_\theta d\theta_{ss}/dV, \\ G_V + G_\theta d\theta_{ss}/dV &= 0, \end{aligned} \tag{A3.1}$$

where F_V, F_θ, G_V, and G_θ are partial derivatives.

On the other hand, the elastodynamic relation (1), noting that $\phi(x, z, t) = 0$ from (5), gives

$$\tau_0^b - (\mu/2c)\, V = \tau_{\text{strength}} = F(V,\theta). \tag{A3.2}$$

Now perturbing (A3.2) by a small change of state variable $\Delta\theta$, and neglecting higher order than linear terms, we have $-(\mu/2c)\Delta V = F_V\Delta V + F_\theta\Delta\theta$ with ΔV being the corresponding variation of velocity and thus related to $\Delta\theta$ by

$$\Delta V = \frac{-F_\theta}{\mu/2c + F_V}\,\Delta\theta. \tag{A3.3}$$

Under this perturbation, let us now examine the tendency of the state variable to change. From (7), again neglecting higher-order terms, we have $\Delta\dot{\theta} = G_V\Delta V + G_\theta\Delta\theta$. Combining with the foregoing equations, we derive

$$\begin{aligned} \Delta\dot{\theta} &= G_\theta\Delta\theta\left[\frac{G_V}{G_\theta}\frac{\Delta V}{\Delta\theta} + 1\right] = G_\theta\Delta\theta\left[\frac{(d\theta_{ss}/dV)F_\theta}{\mu/2c + F_V} + 1\right] \\ &= G_\theta\Delta\theta\left[\frac{d\tau_{ss}/dV - F_V}{\mu/2c + F_V} + 1\right] = \frac{G_\theta(d\tau_{ss}/dV + \mu/2c)}{\mu/2c + F_V}\,\Delta\theta \\ &= -\frac{V}{L}\frac{d\tau_{ss}/dV + \mu/2c}{\mu/2c + F_V}\,\Delta\theta, \end{aligned} \tag{A3.4}$$

where (12) is used in the last step. Recalling that $F_V \geqq 0$, we therefore conclude that small perturbations away from steady-state conditions will decay toward zero when $d\tau_{ss}/dV + \mu/2c > 0$, which is the case for $V = V_{\text{dyna}}$, but will grow to larger value if $d\tau_{ss}/dV + \mu/2c < 0$, which is the case for at least one of any lower-speed solutions as may exist.

Appendix 4

List of Symbols

A, B	direct and evolutionary velocity-dependence parameters in a lab-derived constitutive law
c	shear wave speed
$\delta(x, z, t)$	slip on fault
$\phi(x, z, t)$	a functional of spatially nonuniform slip history $\delta(x, z, t)$
h	element size, or FFT sampling point spacing
h^*	coherent slip patch size
h^*_{B-A}	coherent slip size based on weakening rate $B - A$, $2\mu L/\pi(B - A)$
h^*_{dyna}	coherent slip size based on weakening evaluated at $V = V_{\text{dyna}}$
L (or d_c)	characteristic sliding length in constitutive law
λ	total length of the simulated region along fault, $N_{ele}h$, periodically repeated in space
μ	elastic shear modulus
N_{ele}	total number of elements in the numerical grid
θ	state variable defined in lab-derived constitutive laws
$\sigma_n - p$	effective normal stress
$\tau(x, z, t)$	shear stress
$\tau_0(x, z, t)$	loading stress; would be sustained by the fault if contrained against slip
τ_0^b, τ_0^p	uniform remote background and perturbed levels of the loading stress
τ_{pulse}	stressing level below which no indefinitely expanding crack exists
τ_{arrest}	stressing level at which one gets a steady-state self-healing pulse (and below which the pulse decays with propagation distance)
τ_{strength}	fault strength
$\tau_{ss}(V)$	steady-state fault strength, $\tau_{\text{strength}} = \tau_{ss}(V)$
$\tau_{\text{damp}}(V)$	describes radiation damping line, $\tau_{\text{damp}}(V) = \tau_0^b - \mu V/2c$
$\Delta\tau$	characteristic stress drop of a constitutive law
T	slope ratio between the steady-state strength curve and radiation damping line at V_{dyna}
$V(x, z, t)$	sliding velocity, is equal to $\dot{\delta}(x, z, t)$
V_{dyna}	characteristic velocity in dynamic slip process
V_0, V_{weak}	constants entering different constitutive laws considered

Department of Earth and Planetary Sciences and Division of Engineering and Applied Sciences
Harvard University
Cambridge, Massachusetts 02138

Manuscript received 11 March 1998.